Atmospheric Research 330 (2026) 108580

Contents lists available at ScienceDirect

Atmospheric Research

journal homepage: www.elsevier.com/locate/atmosres

Meteorological conditions and physicochemical processes amplifying ozone pollution during heatwaves in major city clusters of China

Yu Song [a,b], Pinya Wang [a,b,*], Yang Yang [a,b], Jianping Tang [c], Hong Liao [a,b]

[a] State Key Laboratory of Climate System Prediction and Risk Management, Jiangsu Key Laboratory of Atmospheric Environment Monitoring and Pollution Control, Jiangsu Collaborative Innovation Center of Atmospheric Environment and Equipment Technology, Joint International Research Laboratory of Climate and Environment Change, Nanjing University of Information Science and Technology, Nanjing, Jiangsu, China

[b] School of Environmental Science and Engineering, Nanjing University of Information Science and Technology, Nanjing, Jiangsu, China

[c] School of Atmospheric Sciences, Nanjing University, Nanjing, Jiangsu, China

ARTICLE INFO

Keywords:
Heatwaves
Ozone pollution
Meteorological conditions
Physiochemical processes

ABSTRACT

Climate warming has led to a rising frequency of extreme heat events over China, which further exacerbate surface ozone (O_3) pollution alongside accelerating anthropogenic emissions, especially for the key city clusters, i.e., Beijing-Tianjin-Hebei (BTH), Yangtze River Delta (YRD), Sichuan Basin (SCB), and Pearl River Delta (PRD). With long-term observations, reanalysis, and GEOS-Chem simulations, this study reveals significant enhancements ozone levels during heatwave days (HWs) compared to non-heatwave days (NHWs), driven by distinct yet interconnected meteorological and physicochemical processes across different city clusters. In BTH, a persistent 500 hPa high-pressure system, together with reduced relative humidity, enhanced downward solar radiation at the surface, and 850 hPa southerly winds, leads to elevated temperatures and consequently higher O_3 concentrations during HWs compared with NHWs. The YRD experiences intensified subsidence and suppressed cloud cover under the northward shifted Western Pacific Subtropical High (WPSH), creating ideal conditions for photochemistry. Similarly, SCB and PRD, in the dominance of the northwestward extension of WPSH and associated subsidence, features increased SSRD and surface air temperatures. Moreover, tropical cyclones over Northwest Pacific may affect O_3 anomalies in PRD. Process analysis demonstrates that chemical production dominates O_3 enhancement across all regions. Horizontal transport shows a positive contribution in BTH but significant negative contributions in the other three regions. In contrast, vertical transport and mixing processes exhibit relatively weak impacts. The findings can provide theoretical support to tackle ozone pollution for major city clusters in China amid the increasing frequency of extreme heat events.

1. Introduction

Tropospheric ozone (O_3), a typical secondary pollutant, is produced through photochemical reactions with nitrogen oxides (NO_x) and volatile organic compounds (VOCs) released from both natural and anthropogenic sources (Atkinson, 2000; Sillman, 1999; Trainer et al., 2000). Elevated ground-level ozone concentrations pose significant threats to both public health and ecosystems (Booker et al., 2009; Fleming et al., 2018). Cumulative evidence indicates that long-term ozone exposure induces respiratory impairment, elevates cardiovascular disease risks, and exacerbates the incidence of age-related macular degeneration (Arjomandi et al., 2018; Jia et al., 2024; Liu et al., 2022b). Furthermore, as a strong oxidizing pollutant, ozone damages plant cellular structures and physiological functions, substantially dampening crop yield and quality, thereby threatening food security (Feng and Kobayashi, 2009; Feng et al., 2015; Li et al., 2025).

To tackle the severe air pollution challenge in China, the Chinese government has implemented a series of targeted policies since 2013. The Air Pollution Prevention and Control Action Plan and the Blue Sky Defense Battle, as cornerstone initiatives, have established systematic control measures focusing on particulate matter (Wang et al., 2022b). These interventions achieved a notable reduction in population-weighted annual mean fine particle matters ($PM_{2.5}$) concentration from 61.8 μg/m^3 to 42.0 μg/m^3 during 2013–2017 (Zhang et al., 2019).

* Corresponding author at: State Key Laboratory of Climate System Prediction and Risk Management, Jiangsu Key Laboratory of Atmospheric Environment Monitoring and Pollution Control, Jiangsu Collaborative Innovation Center of Atmospheric Environment and Equipment Technology, Joint International Research Laboratory of Climate and Environment Change, Nanjing University of Information Science and Technology, Nanjing, Jiangsu, China.
E-mail address: pinya.wang@nuist.edu.cn (P. Wang).

https://doi.org/10.1016/j.atmosres.2025.108580
Received 20 July 2025; Received in revised form 15 October 2025; Accepted 15 October 2025
Available online 16 October 2025

Despite substantial improvements in $PM_{2.5}$ levels, we are still facing escalating O_3 pollution especially for major city clusters. Yang et al. (2025) systematically analyzed long-term trends of maximum daily 8-h average ozone (MDA8 O_3) concentrations across China, revealing increasing annual trends over 97 % of monitored regions, with coastal southeastern and central plain areas experiencing growth rates exceeding 2 $\mu g/m^3$ per year. The annual increase rate of MDA8 O_3 for warm months reached 2.4 ppb per year nationwide (Lu et al., 2020). Particularly, high ozone concentrations in China typically occur in city clusters, e.g., Beijing-Tianjin-Hebei (BTH), Yangtze River Delta (YRD), Sichuan Basin (SCB), and Pearl River Delta (PRD) (Shu et al., 2016; Zhao et al., 2018; Ouyang et al., 2022).

Simultaneously, China has been particularly affected by increasing and intensifying heatwave events in recent decades, driven by both the global warming and rapid urbanizations (Meehl and Tebaldi, 2004; Lau and Nath, 2014). The year 2024 broke the record of global temperature observations, with the annual mean surface temperature exceeding the pre-industrial level by 1.5$^{\circ}C$ for the first time, while land temperatures exhibited even more pronounced warming, reaching an increase of 2.28$^{\circ}C$ (Jha et al., 2025). Prolonged exposure to such extreme heat can cause substantial increases in mortality rates and socioeconomic loss (Barriopedro et al., 2011). Xie et al. (2024) found that during the period from 1961 to 2020, heatwaves in China resulted in a cumulative excess mortality of 450,000 deaths and caused economic losses of approximately 1284 billion CNY. Projections indicate that heatwaves in China will become more frequent and severe in the future especially under the high-emission scenario (Wang et al., 2017, 2019a; Chen et al., 2022).

Cumulative works have revealed that extreme heat event favor elevated ozone concentrations primarily through enhancing biogenic volatile organic compounds (BVOCs) emissions and accelerating photochemical processes (Kalisa et al., 2018; Varotsos et al., 2019; Wang et al., 2022b). More recently, temperature-dependent emissions of anthropogenic volatile organic compounds (AVOCs) have also been identified as a major contributor to ozone increases during heatwaves (Wu et al., 2024). High temperatures enhance AVOCs release from sources including solvents, industrial activities, and fuel evaporation. This thermally amplified AVOC load intensifies ozone pollution, especially in urban regions (Qin et al., 2025). In addition to the role of near-surface emission sources, turbulent mixing during heatwaves also alters the vertical distribution of ozone precursors, thereby exacerbating ozone pollution both at ground level and in the upper atmosphere (Zhou et al., 2025). Previous works have primarily investigated the ozone responses associated with extreme heat conditions and possible mechanisms based on case studies. For instance, Ma et al. (2019) demonstrated that the notable O_3 increases in North China during summer 2017 was significantly attributable to amplified biogenic emissions induced by extreme heat weather. Similarly, Wang et al. (2024d) investigated a regional ozone pollution episode triggered by persistent heatwaves in the PRD during September 2022. Their findings revealed that elevated temperatures enhanced biogenic volatile organic compound (BVOCs) emissions by approximately 10 %. Wang et al. (2024b) employed the WRF-CMAQ modeling system to assess the Climate Penalty Factor (CPF) in SCB, defined as the ratio of ozone concentration response to temperature changes. They found that the northwestern region of SCB exhibited the highest CPF value with ozone concentrations increasing by 4.12–5.40 ppb/$^{\circ}C$, and the average CPF across SCB increases along higher temperatures, indicating a nonlinear response of ozone concentrations to increasing temperature. Beyond high temperatures, low humidity, intense solar radiation, and weak winds during heatwaves exhibit synergistic effects that collectively enhance ozone accumulation (Ding et al., 2017; Dang et al., 2021). Pu et al. (2017) demonstrated that ozone increases in the YRD during heatwave in 2013 is driven by synergistic effects of enhanced photochemical production and weakened dry deposition. Similarly, a recent study revealed that during the unprecedented August 2022 heatwave, the increase in ozone concentrations in the SCB was also jointly driven by high temperatures, intense solar radiation, and the accumulation of nocturnal pollutants (Wang et al., 2024a). However, such case studies lack comprehensive analysis and spatial comparisons of ozone response to extreme heat across different city clusters.

In this study, we aim to systematically elucidate the meteorological conditions and physicochemical processes governing ozone response during heatwaves across four major Chinese city clusters, i.e., BTH, YRD, SCB, PRD based on long-term surface ozone concentrations for 2014–2023 and meteorological reanalysis and the 3-D global atmospheric chemical transport model GEOS-Chem. The remainder of the paper is organized as follows: Section 2 describes the methodology and datasets; Section 3.1 presents spatiotemporal characteristics of heatwave indices and MDA8 O_3 across China; Section 3.2 examines ozone anomaly patterns during heatwaves in the four city clusters; Section 3.3 analyzes anomalous atmospheric circulation and meteorological factors during heatwave events; and Section 3.4 quantifies the physicochemical processes underlying ozone anomalies through GEOS-Chem simulations. Summary remarks are provided in Section 4.

2. Data and methods

2.1. Surface ozone concentrations

Hourly ozone (O_3) concentrations from 2014 to 2023 are obtained from the China National Environmental Monitoring Center (CNEMC). The monitoring network expanded from 944 sites in 2014 to approximately 1800 sites by 2023, representing the most comprehensive ground-level ozone dataset in China. Following established protocols (Li et al., 2004), the raw data underwent rigorous quality control, including instrument calibration, outlier removal, and continuity checks. This dataset has been widely used in previous studies of the impact of heatwave on ozone (Wang et al., 2019b; You et al., 2017). To facilitate regional-scale analysis, the observational data are interpolated onto a $1^{\circ} \times 1^{\circ}$grid, with each grid cell value representing the average of all station observations within its boundaries.

2.2. Meteorological reanalysis datasets

This study utilizes meteorological variables obtained from the fifth generation of the European Centre for Medium-Range Weather Forecasts (ECMWF) reanalysis data (ERA5) for the period 1960–2023. The data are extracted at 00:00, 06:00, 12:00, and 18:00 UTC daily from May to September each year, with a horizontal resolution of $0.25^{\circ} \times 0.25^{\circ}$. The selected variables include geopotential height (HGT) and wind fields at 500 hPa and 850 hPa, surface solar radiation downwards (SSRD), total cloud cover (TCC), 2-m air temperature (T2m) and dew point temperature. Relative humidity (RH) is calculated using T2m and dew point temperature. Note that daily mean (maximum) values of different variables are obtained as the average (maximum) of four records per day for subsequent analysis.

2.3. Definition and indices of heatwaves

Heatwave events (HWs) can be divided into two types according to their criteria of high temperatures, i.e., the absolute heatwaves based on fixed temperature thresholds and the relative heatwaves based on the percentile-based thresholds (Perkins and Alexander, 2013; IPCC, 2023). Specifically, absolute heatwaves typically employ a fixed threshold for high temperature, e.g., daily maximum temperature (Tmax) $\geq 35^{\circ}C$ (Tong et al., 2010; Wang et al., 2012) while the relative heatwaves generally adopt the local climatological percentiles, e.g., the 95th percentile of daily temperature series (Li et al., 2024a). Considering the notable climatological heterogeneity across China, we adopted a relative threshold approach to define heatwaves. The climatological baseline period was set to 1961–1990. For each calendar date, the 90th percentile

threshold (Tmax_90th) of Tmax was calculated using a 15-day centered moving window, resulting in a pool of 450 daily values (30 years × 15 days). HWs were identified as periods of at least three consecutive days during which daily Tmax exceeded the corresponding Tmax_90th. HW days refer to all days within HW events. And the non-heatwave days (NHWs) comprising all days during May–September excluding HW days. It is worth noting that using a higher threshold, i.e., the 95th percentile of daily maximum temperature for heatwave identification would reduce the number of heatwave days but would not alter the observed enhancement of surface ozone during heatwave periods (Fig. S1).

Following Wang et al. (2017), four key heatwave indices are used to characterize HWs: heatwave number (HWN) is quantified as the annual count of heatwave events; heatwave duration (HWDU) is calculated as average duration of heat waves within a year; heatwave magnitude (HWM) measures the mean magnitude of temperature exceedances relative to its corresponding threshold during heatwave periods; and heatwave frequency (HWF) represent the yearly sum of participating heat wave days.

As exposure to high ozone concentrations pose a severe threat to human health, we further assess the impacts of HWs on ozone pollution days (OPDs), defined as days when daily MDA8 O_3 concentrations greater than 80 ppb (around 160 μg/m^3). Table 1 gives the key metrics of OPDs during HWs and NHWs respectively, including OP days, intensity of ozone pollution (OPI), and probability ratio (PR) of OPDs. The OPI means the mean MDA8 O_3 concentrations during OPDs and PR indicate the OPDs relative to all HW days for a specific region. Higher PR values indicate a higher risk of ozone pollution during HWs.

2.4. GEOS-Chem simulations

The GEOS-Chem model (Version 13.4.1), a three-dimensional global chemical transport model, is employed to simulate surface O_3 variability and investigate key chemical and dynamical processes driving its distribution from 2014 to 2023. The experiments are conducted at a horizontal resolution of 0.5°latitude× 0.625°longitude with the boundary conditions from a global GEOS-Chem simulation at 2°latitude × 2.5°longitude resolution with 47 vertical levels extending from the surface to 0.01 hPa. GEOS-Chem v13.4.1 incorporates a fully coupled O_3-NO_x-hydrocarbon-aerosol chemical mechanism (Pye et al., 2009; Mao et al., 2013; Sherwen et al., 2016), which enables comprehensive simulations of ozone and other gaseous pollutants along with aerosols. The meteorological fields are driven by the Modern-Era Retrospective Analysis for Research and Applications, Version 2 (MERRA-2; Gelaro et al., 2017) reanalysis dataset. Note that the simulated heatwaves are identified based on daily maximum air temperature from MERRA2 that are used to drive GEOS-Chem.

The global anthropogenic emissions data used in this study, including ozone precursors (CO, NO_x, and non-methane volatile organic compounds (NMVOCs), are sourced from the Community Emissions Data System (CEDS v_2021_04_21; Hoesly et al., 2018). Regarding the selection of emission inventory, the Community Emissions Data System (CEDS v_2021_04_21) adopted in this study has updated the anthropogenic aerosols and precursors emissions with country-level emission inventories of China, Europe and North America (Gao et al., 2023; Li et al., 2023). Besides, the model evaluation shows a reasonable agreement with observed ozone concentration responses during heatwaves, supporting its applicability. This study conducts GEOS-Chem simulations from 2014 to 2023. Following a six-month spin-up period, the simulations were performed with anthropogenic emissions held constant at 2019 levels. We adopted fixed anthropogenic emissions to isolate the response of surface ozone concentrations driven solely by changes in meteorological conditions. This approach is a common practice in previous studies (Li et al., 2024b; Ni et al., 2024). Methane (CH_4) background concentrations are provided by the Global Monitoring Laboratory (GML) of the National Oceanic and Atmospheric Administration (NOAA). Biomass burning emissions are derived from Version 4 of the Global Fire Emissions Database (GFED4; Van der Werf et al., 2017). Stratospheric ozone chemistry adopts the LINOZ scheme (McLinden et al., 2000). The emissions of BVOC components are calculated online using the Model of Emissions of Gases and Aerosols from Nature, Version 2.1 (MEGAN v2.1; Guenther et al., 2012). MEGAN2.1 estimates emissions (Fi) of chemical species i from terrestrial landscapes as the product of these two components in units of (μg m^{-2} h^{-1}) for 19 compound classes (i) according to

$$F_i = \gamma_i \sum \varepsilon_{i,j} \chi_j \quad (1)$$

where $\varepsilon_{i,j}$ is the emission factor at standard conditions for vegetation type j with fractional grid box areal coverage χ_j. The emission activity factor (γ_i) accounts for the major processes controlling emission responses to environmental and phenological conditions, which accounts for emission response to light (γP), temperature (γT), leaf age (γA), soil moisture (γSM), leaf area index (LAI) and CO_2 inhibition (γC). Among these processes, γ_i exhibits an exponentially increasing response to temperature, a piecewise linear response to soil moisture and a light dependent response that is generally linear under low radiation level but reach a constant at high radiation levels.

The GEOS-Chem model with identical parameterization schemes has been extensively validated for simulating O_3 spatial distributions. Multiple independent studies have demonstrated its exceptional capability in reproducing both observed ozone concentrations and spatial patterns across China (Yang et al., 2014, 2022) and reliably characterizes regional distribution features (Ni et al., 2018; Li et al., 2019; Lu et al., 2019). These systematic validation efforts confirm the model's applicability and reliability for Chinese regional studies.

Table 1
Key metrics of ozone pollution during HWs and NHWs for the four city clusters.

		BTH	YRD	SCB	PRD
HWs	OPDs (days)	94	75	49	61
	OPI (ppb)	90.88	80.84	74.83	57.90
	PR (%)	76	47	32	17
NHWs	OPDs (days)	472	245	67	75
	OPI (ppb)	72.99	63.33	55.05	47.13
	PR (%)	34	18	5	11

3. Results

3.1. Spatial-temporal patterns of heatwave indices and MDA8 O_3 in China

To characterize the long-term evolution of heatwave characteristics and ground-level ozone, we first examine the four heatwave indices across China for the warm season (May–September) from 1960 to 2023. Fig. 1 presents the spatial distributions of four heatwave indices across China during 1960–2023. As we can see, HWN and HWDU reveal pronounced maxima in SCB, YRD, and southeastern coastal provinces, with HWN exceeding 15 days and HWDU dominated by multi-day events (>4 days), corresponding to regions of high humidity and persistent subtropical high influence (Fig. 1a–b). In contrast, HWM, defined as the average temperature exceedance above the 90th percentile threshold, peaks in BTH and along the SCB and YRD regions. (Fig. 1c). HWF exhibits a spatial pattern like HWN, being most prominent in SCB, YRD, and southeastern coastal provinces with values exceeding 3 events (Fig. 1d). These patterns underscore the interplay between synoptic-scale circulation and local topography in modulating heatwave characteristics.

The annual evolution of heatwave indices over the main city clusters during 1960–2023 are demonstrated in Fig. 2. All indices exhibited relatively stable trends with minor fluctuations prior to 1990, followed by significant upward trends thereafter, particularly since 2010s. For

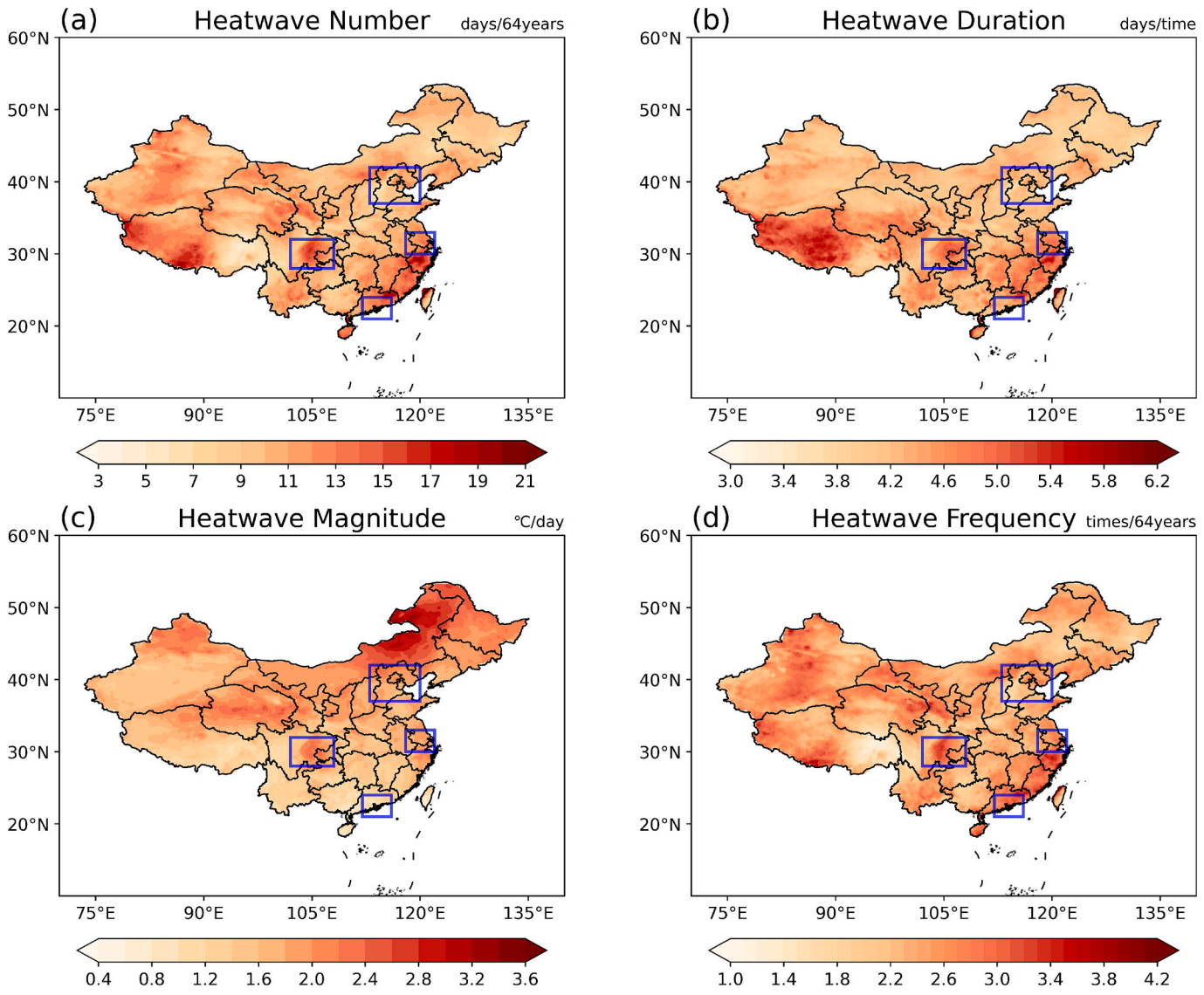

Fig. 1. Spatial patterns of (a) heatwave number (HWN), (b) heatwave duration (HWDU), (c) heatwave magnitude (HWM), and (d) heatwave frequency (HWF) over China for May–September during 1960–2023. The blue box in each panel indicates the following regions: Beijing-Tianjin-Hebei (BTH; 37–42°N, 113–120°E), Yangtze River Delta (YRD; 30–33°N, 118–122°E), Sichuan Basin (SCB; 28–32°N, 102–108°E), and Pearl River Delta (PRD; 21–24°N, 112–116°E). (For interpretation of the references to colour in this figure legend, the reader is referred to the web version of this article.)

heatwave number (HWN, Fig. 2a), the PRD showed the most rapid increase (0.67 days/year), followed by the YRD, while BTH and SCB regions displayed comparable but lower growth rates. The PRD also exhibited the fastest growth in both HWF (0.10 times/year) and HWDU (0.04 days/year), approximately double the rates observed in the other three regions (Fig. 2b–c). Regarding HWM, all regions showed similar increasing trends, with YRD and PRD warming at 0.61°*C*/year, slightly higher than BTH and SCB (0.55°*C*/year) (Fig. 2d).

As illustrated in Fig. 2, all four heatwave indices across China exhibited exceptionally rapid increases from 2014 to 2023, a period characterized by intensified ozone pollution (Wang et al., 2022a). Fig. 3 displays the spatial distribution of the maximum MDA8 O_3 concentrations and their linear trends for the warm season (May–September) from 2014 to 2023 over China. Over the past decade, BTH region has experienced the most severe ozone pollution in China due to intensive heavy industrial activities emitting large amounts of ozone precursors (Yang et al., 2025), with peak MDA8 O_3 exceeding 150 ppb in BTH, followed by YRD, SDB and PRD. Moreover, most regions in China experience an annual increase trend in MDA8 O_3, with maxima over BTH (up to 5 ppb/yr), exceeding the earlier reported trend of 3.1 ppb/yr for 2013–2017 (Li et al., 2019). Similar growth rates were observed in YRD (0.19–3.53 ppb/yr) and SCB (0.11–3.14 ppb/yr), while PRD with a rate between −1.1–0.94 ppb/yr. These hotspots of increasing ozone pollution correlate closely with rapid urbanization over the four major city clusters.

The annual variations regional mean MDA8 O_3 indicate that BTH and YRD exhibited comparable growth rates (~1.7 ppb/yr), followed by SCB (~1.33 ppb/yr), while PRD had the lowest increase (~0.53 ppb/yr) (Fig. 4). Notably, all regions peaked around 2019, likely due to declining NO_2 levels promoting ozone accumulation (Yang et al., 2025). Post-2019, near-surface ozone concentrations generally declined across China, potentially tied to anthropogenic controls and the COVID-19 lockdowns (Yin et al., 2021; Steinbrecht et al., 2021). The Blue Sky Defense Battle implemented during 2018–2021 effectively reduced ozone pollution through sustained emission control measures (Wang et al., 2023b; Yan et al., 2024). In particular, ozone concentration levels cross four city clusters in China exhibited a significant rebound in 2021 and 2022, primarily driven by the record-breaking extreme heatwaves (Wang et al., 2025a; Yan et al., 2024).

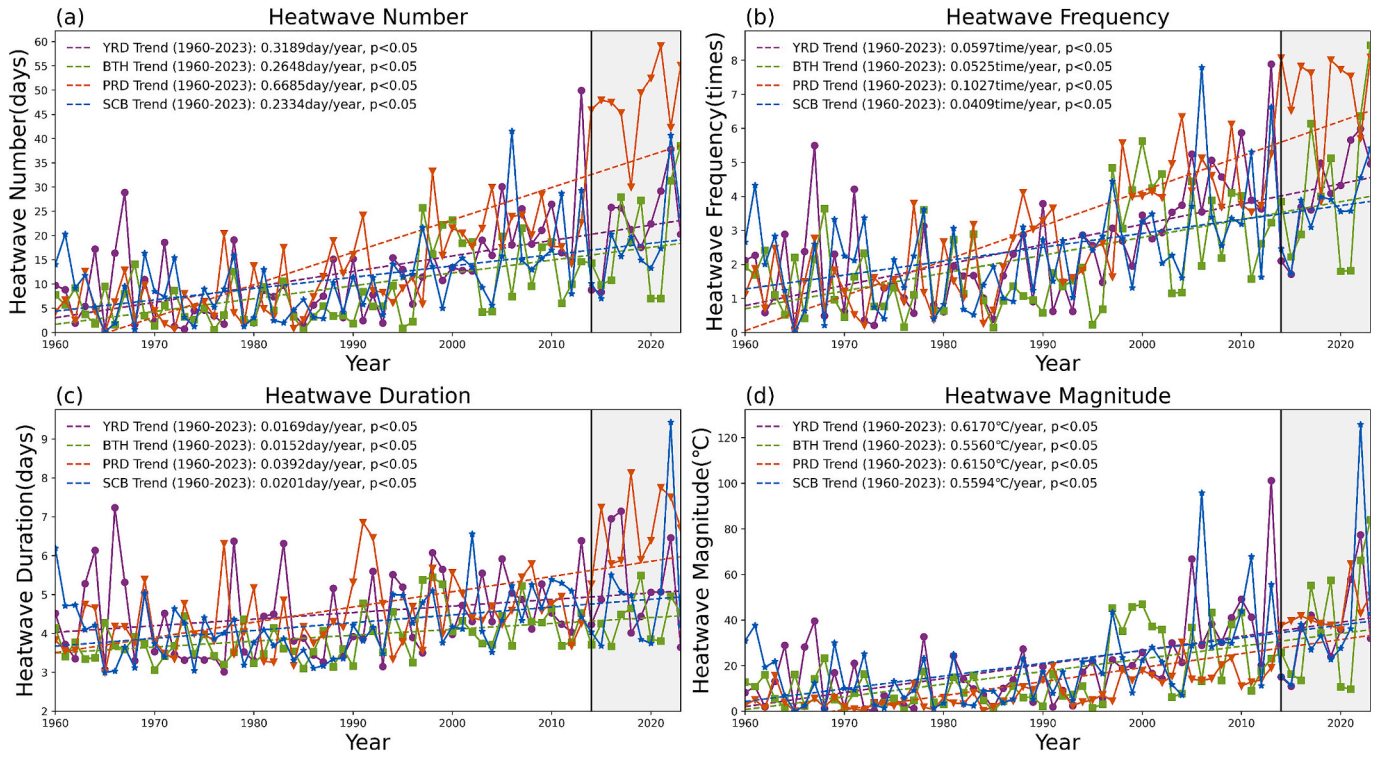

Fig. 2. Interannual variations and linear trends of heatwaves indices during May–September of 1960–2023 across four main city clusters: (a) heatwave number, (b) heatwave frequency, (c) heatwave duration, and (d) heatwave magnitude. Dashed lines indicate linear trends, with regression slopes shown near the top of each panel. Gray shading highlights the period of 2014–2023.

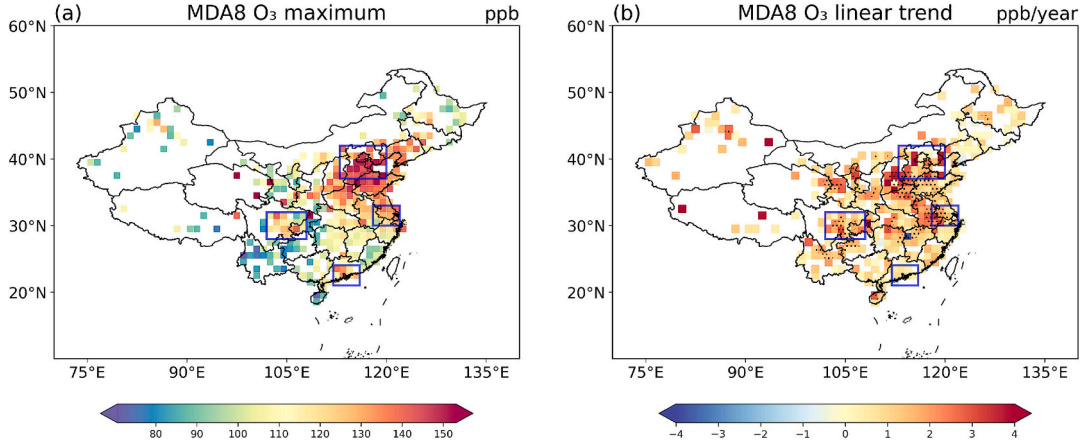

Fig. 3. Spatial distributions of (a) summer (May–September) peak MDA8 O_3 (ppb) and (b) their linear trends (ppb/year) during 2014–2023. Black dots in both panels indicate grid cells with trends significant at $p < 0.05$ (Student's *t*-test). The blue box in each panel indicates the four city clusters. (For interpretation of the references to colour in this figure legend, the reader is referred to the web version of this article.)

3.2. Enhancements in ozone concentrations over major city clusters during HWs

Elevated surface ozone concentrations during heatwave episodes are previously emphasized based on case studies (Gong and Liao, 2019; Wang et al., 2022b). Here, we systematically examine the ozone concentrations changes during heatwave events across China with a long period of focus from 2014 to 2023. Fig. 5 displays the surface ozone concentration anomalies during HWs (2014–2023) relative to NHWs over the four city clusters (BTH, YRD, SCB, and PRD). Elevated ozone levels are observed during heatwaves across all regions, with anomalies exceeding 20 ppb centered over all city clusters. Among the four city clusters, the BTH region demonstrates the strongest MDA8 O_3 increases, which is likely driven by the most abundant anthropogenic emissions (Dang et al., 2021). Moreover, with the ozone chemical regime gradually shifts from VOC-limited to transitional regimes in China since the continuous clean actions, the increased BVOCs during heatwaves can effectively boost ozone pollution trough enhanced photochemical production (Zhu et al., 2023; Yan et al., 2024).

We further differentiate heatwave events into dry and wet types based on relative humidity thresholds, following Ding and Ke (2015). A threshold of 60 % is applied to classify dry heatwaves (DHWs; RH $<$ 60 %) and wet heatwaves (WHWs; RH $\geq$ 60 %) in the BTH, YRD, and SCB regions. Given that the PRD region is characterized by persistently high relative humidity, and the 60 % threshold fails to capture any DHWs, we adjust the threshold to 80 % for PRD which enables the identification of

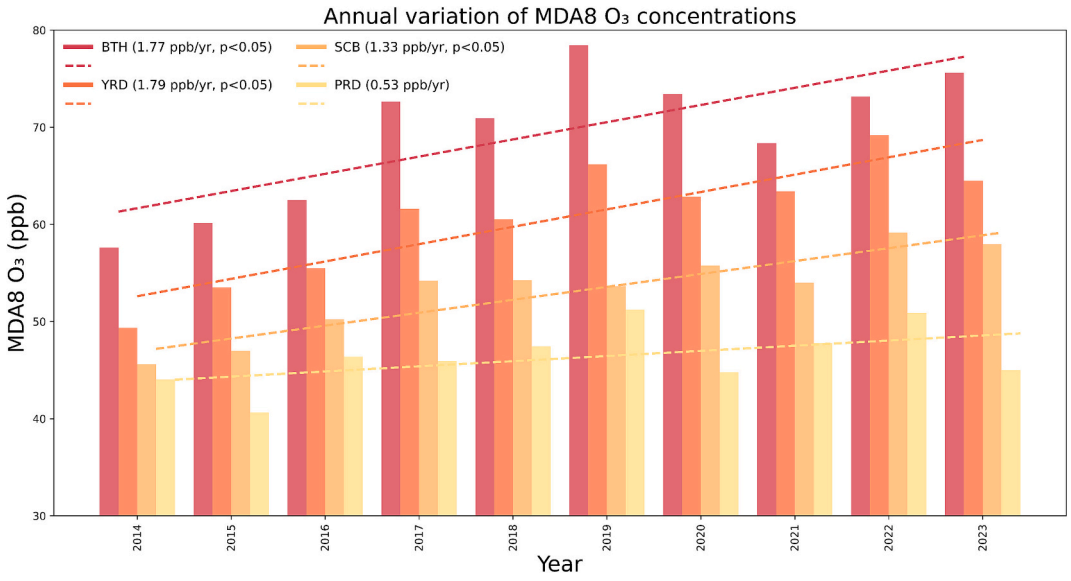

Fig. 4. Annual variation of MDA8 O_3 concentrations during May–September of 2014–2023 for BTH, YRD, SCB, and PRD.

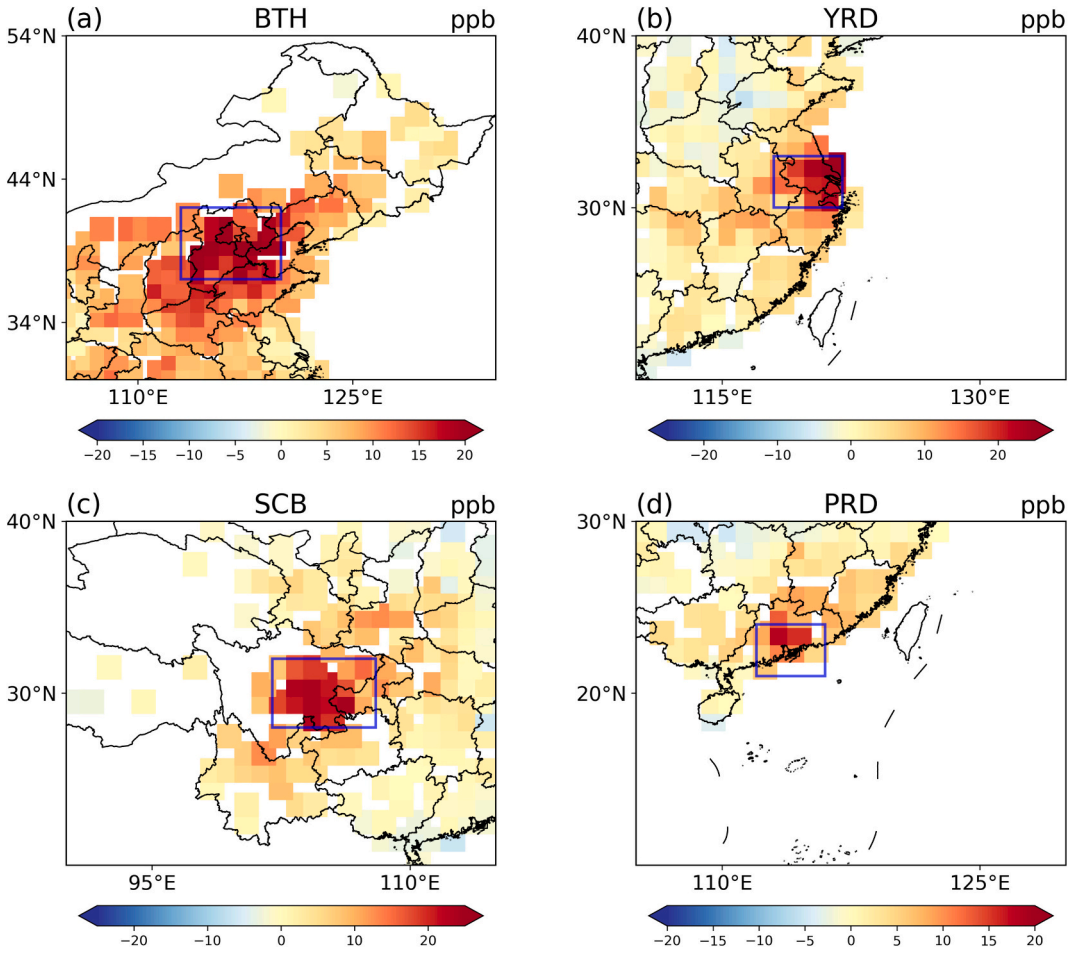

Fig. 5. Differences in MDA8 O_3 between HWs and NHWs for the four city clusters. The BTH, YRD, SCB, and PRD regions are outlined in each panel.

both WHWs and DHWs. Our analysis shows that DHWs generally exhibit higher surface ozone concentrations than WHWs (Fig. S2), highlighting the critical role of humidity in modulating the ozone–heatwave relationship across different urban clusters. The result is consistent with previous work that during DHWs, the drought stress trigger plants close their stomata to reduce water loss, limiting the uptake of ozone by vegetation, a component of dry deposition, and thereby increasing surface ozone concentrations (Lin et al., 2020).

It's clear that BTH shows higher OPDs across the four city clusters, followed by YRD, PRD and SCB in both HW and NHW days. Note that

OPI is elevated during HWs compared to NHWs, with OPI increasing from 72.99 ppb to 90.88 ppb for BTH, from 63.33 ppb to 80.84 ppb for YRD, from 55.05 ppb to 74.83 ppb for SCB and from 47.13 ppb to 57.90 ppb for PRD. Accordingly, PR values are higher during HWs than NHWs, with increases of 42 % for BTH, 29 % for YRD, 27 % for SCB, and 6 % for PRD compared to NHW periods. Note that BTH recorded the highest OPI (90.88 ppb) while PRD had the lowest (57.90 ppb), consistent with the spatial distributions of average ozone concentrations.

3.3. *Anomalous meteorological conditions during HW days compared to NHW days*

To elucidate the role of synoptic circulation in modulating the ozone anomalies during HWs relative to NHWs, we further assess the differences in key meteorological variables between HW and NHW days. Figs. 6 to 9 demonstrate the differences in meteorological conditions between HW and NHW days across four major city clusters, respectively.

As shown in Fig. 6, for BTH region during HW days compared to NHW days, anomalous positive 500 hPa geopotential height anomalies with an anticyclonic circulation dominate the northeast of BTH (Fig. 6a). Subsidence under this high-pressure system significantly reduces RH (Fig. 6c) and TCC (Fig. 6b), thus enhance SSRD (Fig. 6e) and near-surface heating (Fig. 6f). The 850 hPa level also exhibits anomalous high-pressure system and an anticyclonic circulation, with southerly anomalies. Such synoptic pattern, characterized by high pressure and southerlies has been found to favor the occurrences of ozone pollution over North China plain (Gong and Liao, 2019), support our findings.

For the YRD region during HW days compared to NHW days, pronounced positive geopotential height anomalies at 500 hPa accompanied by anticyclonic circulation anomalies are observed over Shandong Province and adjacent maritime areas to the north of YRD (Fig. 7a). This pattern indicates an abnormally intensified and northward shifted WPSH, extending beyond 30°N. At 850 hPa, the positive anomaly center is located over the eastern maritime areas of the Yangtze River Delta, accompanied by anticyclone circulation (Fig. 7d). Such high-pressure system further enhances subsidence, lead to depressed TCC and RH while and increased SSRD and T2m. The results are consistent with Jiang et al. (2021) that the WPSH serves as a crucial circulation system driving heatwaves in eastern China.

For the anomalous synoptic circulation over SCB during HW days compared to NHW days, the widespread positive geopotential height anomalies north of 30°N at 500 hPa (Fig. 8a) indicate an anomalously intensified and northwestward extended WPSH, which significantly contributed to subsidence, which leads to depressed convection and reduced TCC (Fig. 8b), thus enhanced SSRD (Fig. 8e) and elevated T2m (Fig. 8f). At the lower level of 850 hPa, the negative geopotential height anomalies reflected thermally induced surface low pressure, with weak positive anomalies on the western side enhancing subsidence (Fig. 8d). Although southerly winds at 850 hPa transported moist air, the prevailing subsidence would decrease RH (Fig. 8c).

Compared to NHW days, PRD region during HW days, is dominated by positive geopotential height anomalies at 500 hPa, which covers most of China (Fig. 9a). Such positive GHT anomalies are associated with intensified and the westward extension of the WPSH, characterized by deep subsidence, thus favoring less TCC (Fig. 9b) and increased SSRD and T2m (Fig. 9e & f). At the lower level of 850 hPa, an anticyclonic circulation with weak positive geopotential height anomalies is observed west flank the PRD region, while a low-pressure center and cyclonic circulation appear over the eastern flank of PRD, likely associated with tropical cyclone (TC) activities (Fig. 9d). The anomalous northerly winds prevail over PRD, suppress moisture transport to PRD, contributing to decreased RH (Fig. 9c). Such phenomenon during heatwaves has been discussed by Luo and Lau (2017). It's have been previously documented that tropical cyclones trigger north shift of WPSH (Wang et al., 2023a). Moreover, for PRD region during simultaneous HWs and OP days, the 850 hPa low-pressure system is more

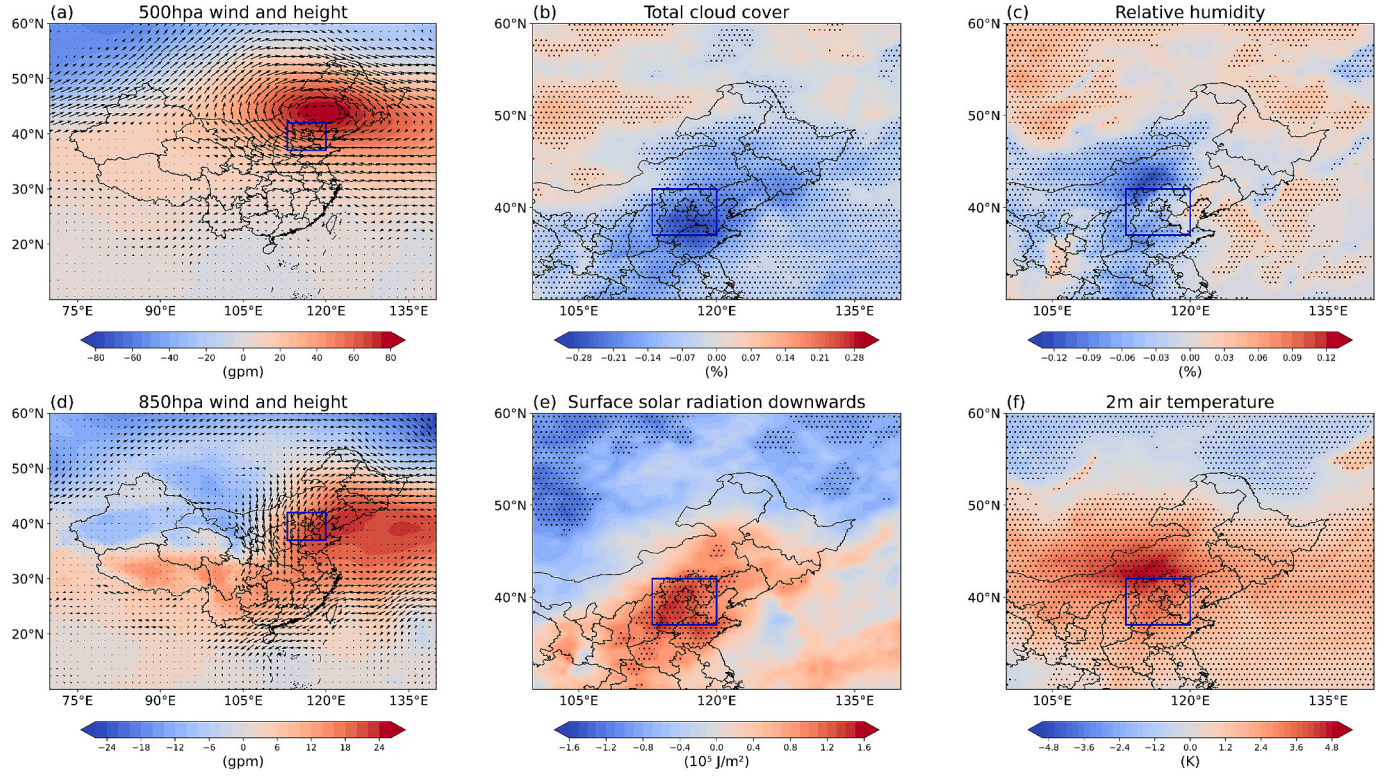

Fig. 6. Spatial distributions of composite anomalies computed as HWs minus NHWs differences in the BTH region: (a) wind field and geopotential height at 500 hPa, (b) total cloud cover (TCC), (c) relative humidity (RH), (d) wind field and geopotential height at 850 hPa, (e) surface solar radiation downwards (SSRD), (f) 2 m air temperature (T2m). Black dots indicate statistically significant anomalies at the 95 % confidence level.

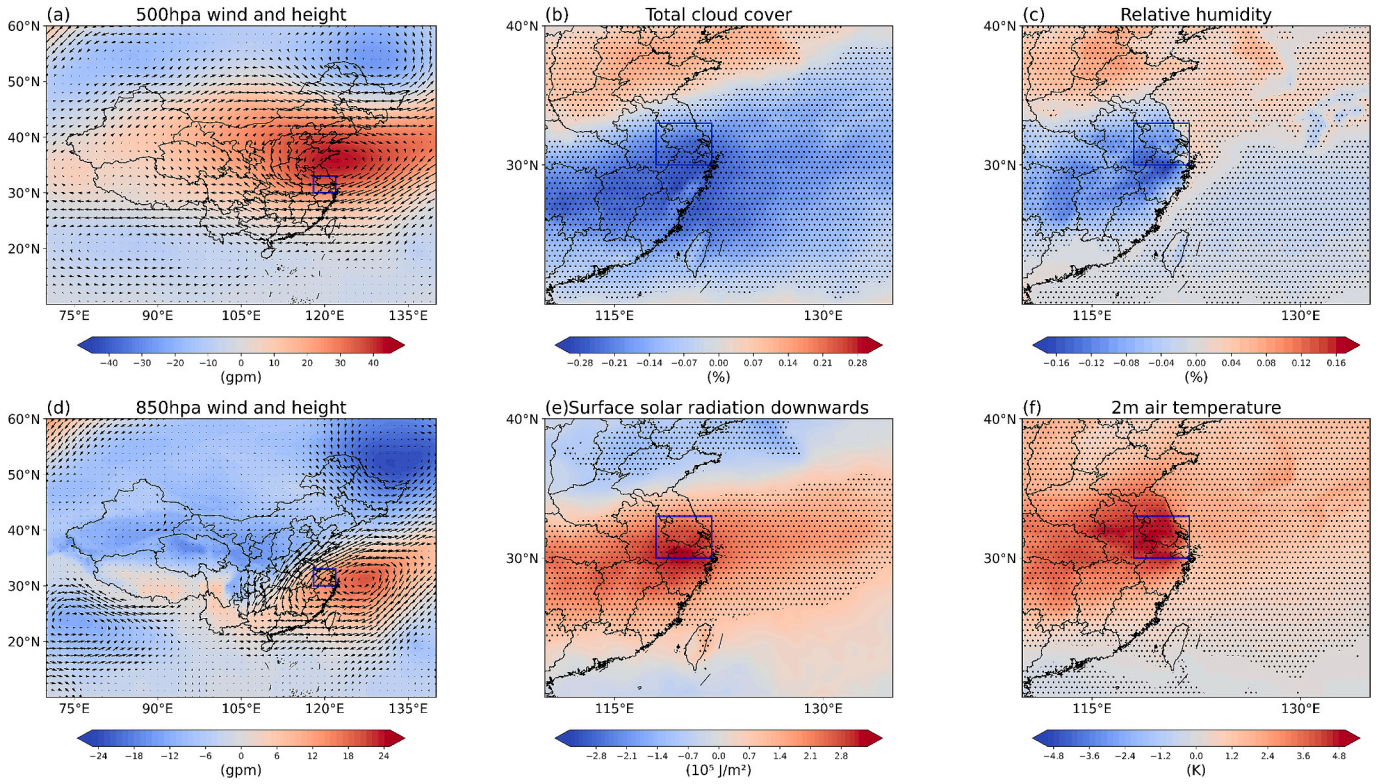

Fig. 7. Same as Fig. 6 but for the YRD region.

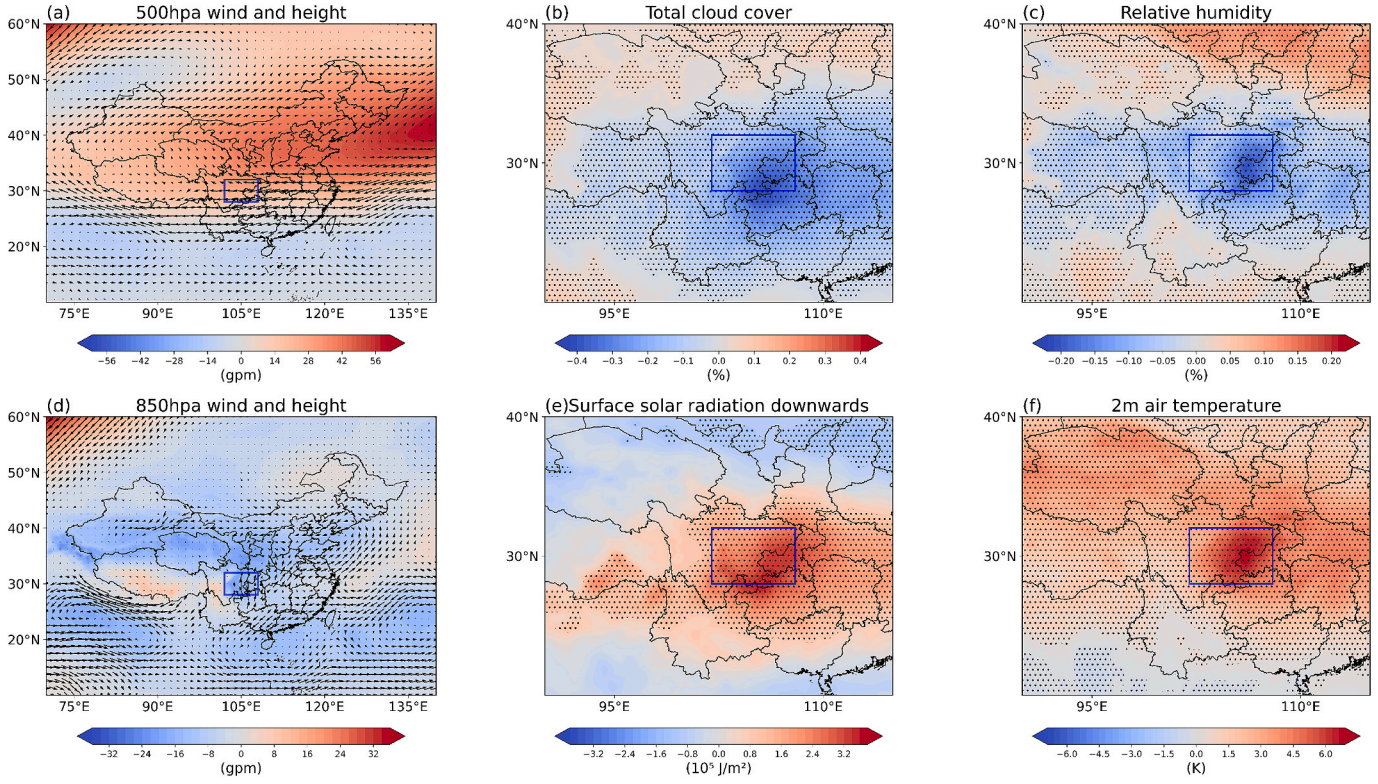

Fig. 8. Same as Fig. 6 but for the SCB region.

pronounced, indicating more notable typhoon activity (Fig. S6). The strong northerly land winds can increase ozone pollution over PRD through cross-section transport (Qi et al., 2024).

Note that for each of the four major city clusters, the synoptic circulation anomalies during the concurrent occurrences of HWs and OP days compared to NHWs demonstrate similar spatial patterns but with

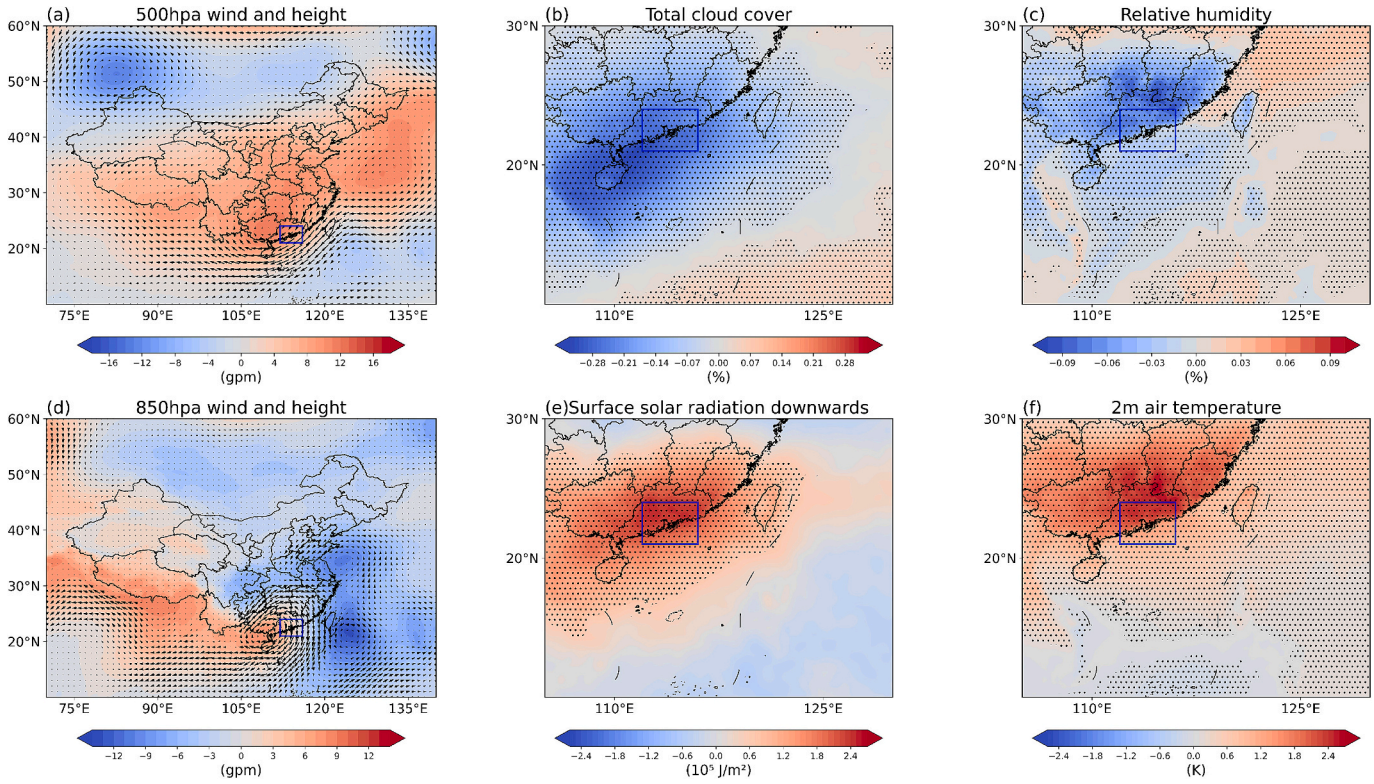

Fig. 9. Same as Fig. 6 but for the PRD region.

stronger magnitude (Figs. S3–S6), consistent with Wang et al., 2022b that meteorological conditions during co-occurrences of heat extreme and OP days are more conducive to ozone pollution than those during extreme heat days alone.

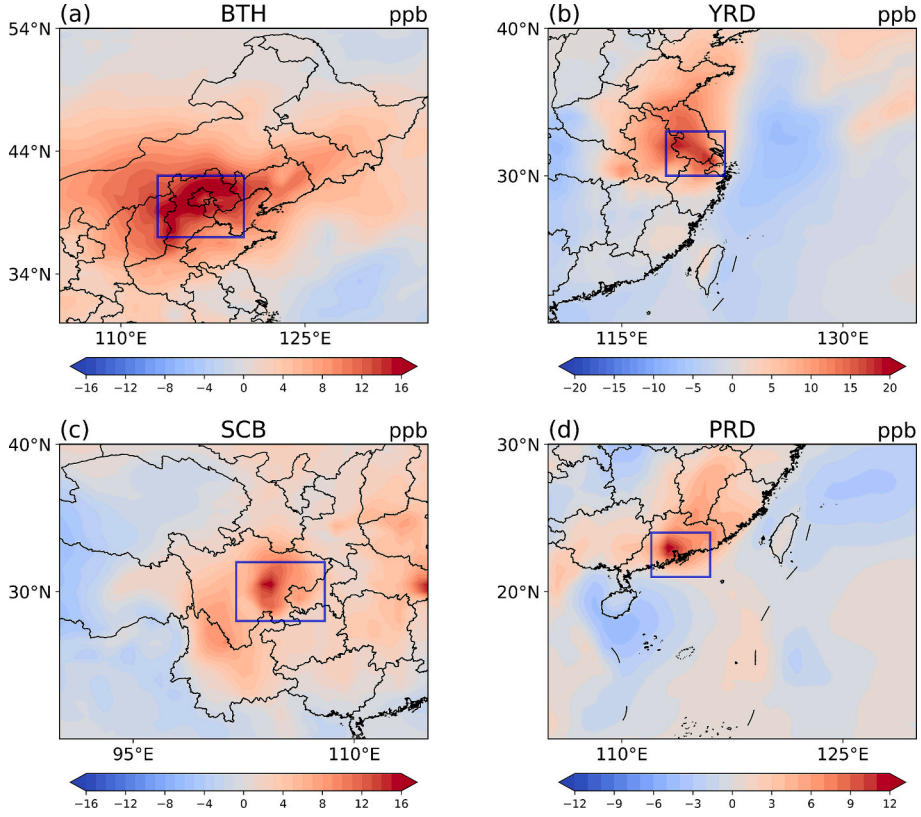

Fig. 10. Same as Fig. 5 but based on GEOS-Chem simulation results.

3.4. Physiochemical process analysis with GEOS-Chem simulations

To quantify the contribution of individual processes, we conduct a process analysis in GEOS-Chem, evaluating the roles of different physiochemical processes in modulating surface ozone concentrations during HWs across the major city clusters. Firstly, we validate the capacity of GEOS-Chem in reproducing ozone concentrations by comparing simulated and observed spatial patterns of surface MDA8 O_3 anomalies during HWs (Fig. 10). The model can capture the characteristic spatial gradients of ozone enhancements, with simulated average anomalies of 18 ppb for BTH, 16 ppb for YRD, 14 ppb for SCB, and 12 ppb for PRD, respectively. Thus, GEOS-Chem successfully reproduced elevated MDA8 O_3 concentrations during HWs across all regions, consistent with observation (as shown in Fig. 5).

We further investigated the key physicochemical processes governing ozone variability, including net chemical production, vertical advection, horizontal advection, and mixing (the combined effect of dry deposition and diffusion). Fig. 11 presents vertical profiles of each process anomalies during HWs relative to NHWs for BTH, YRD, SCB, and PRD, respectively. Over the BTH region as shown in Fig. 11a, chemical production is the dominant driver of ozone enhancement from the surface to 800 hPa, driven by high temperatures and intense solar radiation (Fig. 6e & f). Meanwhile, horizontal transport driven by anomalous southerlies (Fig. 6d) shows a positive contribution from surface to mid-troposphere. In contrast, mixing and vertical advection generally reduce surface ozone concentration from surface to 850 hPa. The YRD and SCB exhibit similar patterns with chemical production contributing positively throughout from surface to 500 hPa (Fig. 11b–c), driven by the elevated temperatures and strong solar radiation during heatwaves (Figs. 7 & 8). Concurrently, high temperatures and the strong radiation may intensify surface ozone concentration through chemical production while horizontal transport associated with strong winds tend to reduce ozone concentration from surface to 500 hPa. Similarly, for PRD, the chemical production process is the dominant driver to ozone enhancements from surface to 850 hPa whereas horizontal transport and vertical transport tends to reduce ozone levels.

Table 2 reveals that chemical production is the predominant factor for ozone enhancement across all four city clusters. Horizontal transport demonstrates substantial regional variability, showing a 38 % positive contribution in BTH but significant negative contributions in other regions, particularly notable in YRD (−52 %) and SCB (−53 %). Vertical transport and mixing processes exhibit relatively minor impacts, generally between −10 % ~ 10 %. The findings highlight that, in addition to local emissions, cross-regional transport plays a pivotal role in shaping ozone pollution across city clusters, underscoring the need for coordinated regional control strategies to achieve effective mitigation. Note that elevated temperatures have been reported to enhance BVOC emissions, which in turn accelerate photochemical reactions and exacerbate ozone pollution (Wang et al., 2024c). As shown in Fig. S7, BVOC emissions (isoprene) are generally higher during heatwaves compared with non-heatwave periods. Moreover, with the O_3 chemical regime gradually shifts from VOC-limited to transitional regimes in China since the continuous clean actions, the increased BVOCs during heatwaves can effectively boost ozone pollution trough enhanced photochemical production (Zhu et al., 2023; Yan et al., 2024).

Table 2
Contributions (%) of different processes to anomalous ozone mass from the surface to 500 hPa during HWs relative to NHWs for the four city clusters.

	Chemistry	Convection	Mixing	Transport
BTH	46 %	−6 %	−10 %	38 %
YRD	48 %	0 %	0 %	−52 %
SCB	41 %	6 %	0 %	−53 %
PRD	63 %	−12 %	0 %	−25 %

The changes in horizontal ozone mass fluxes from the surface to 850 hPa over the four city clusters simulated by the GEOS-Chem model are further shown in Fig. 12. Overall, the BTH region is characterized by pronounced net inflows of O_3 mass fluxes, primarily from the southern boundary (26.03 Gg/d), indicating that regional transport substantially enhances local ozone levels during HWs. In contrast, the YRD and SCB regions both exhibit net outflows of O_3 mass fluxes, which is are dominated by strong outflow along the along their northern boundaries, i.e., 23.58 Gg/d and 25.51 Gg/d, respectively. PRD also exhibit net outflows of ozone mass fluxes, primarily dominated by an outflow at the southern boundary (8.33 Gg/d). These contrasting transport behaviors across regions highlight the heterogeneous role of boundary ozone fluxes in modulating surface ozone concentrations during HWs, with BTH being most strongly influenced by external import, while YRD, PRD and SCB are more sensitive to local accumulation and subsequent export.

4. Discussion and conclusions

In recent years, while stringent air pollution control measures in China have led to a decline in $PM_{2.5}$ concentrations, ground-level ozone levels have exhibited a persistent upward trend. Global warming, on the other hand, has led to increasing occurrences of heat extremes. Extreme high temperatures can amplify ozone pollution, particularly in the four most densely populated city clusters, e.g., BTH, YRD, SCB, and PRD. This

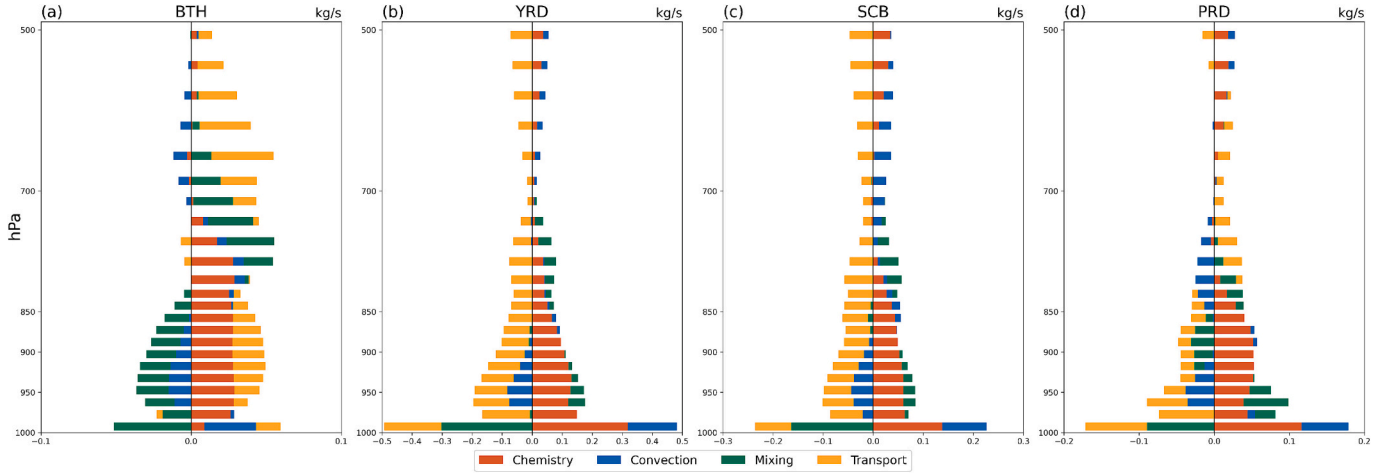

Fig. 11. Vertical profiles of net changes in ozone mass (kg/s) anomalies (HWs minus NHWs) during May–September 2014–2023 for (a) BTH, (b) YRD, (c) SCB, (d) PRD.

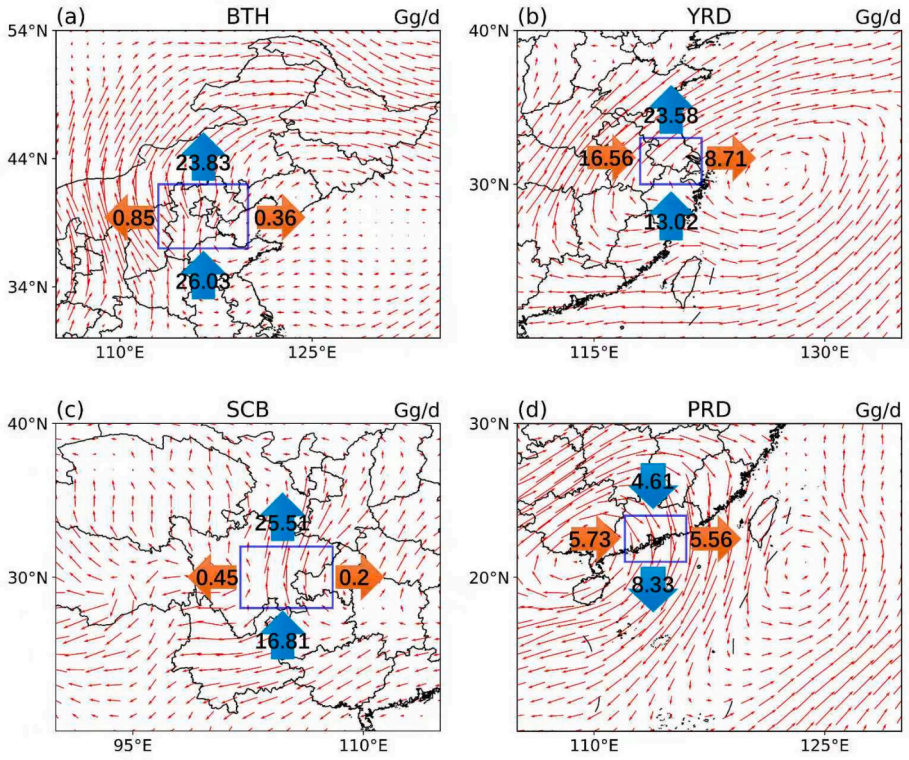

Fig. 12. Composite differences in the horizontal ozone mass fluxes (Gg/d) integrated from the surface to 850 hPa along the boundaries between HWs and NHWs for the four city clusters.

study systematically analyzes the meteorological conditions and associated physiochemical processes driving ozone responses during HWs in the major city clusters by integrating ozone observation data with the ERA5 reanalysis dataset as well as the GEOS-Chem simulation.

The results reveal that, compared to NHWs, all four city clusters experience pronounced increases in surface ozone concentrations during HWs, with maxima exceeding 20 ppb. Meteorological analyses indicate that BTH is predominantly influenced by an anomalous 500 hPa high-pressure system coupled with southerly winds at 850 hPa. YRD is directly impacted by the northward-shifted WPSH, where subsidence, clear skies, low humidity, and intensified solar radiation can synergistically enhance photochemical reactions. SCB is controlled by a northwestward extended WPSH, along with strong subsidence and increased solar radiation. PRD, also under WPSH dominance at 500 hPa, features an 850 hPa anticyclonic circulation and anomalous northerlies that inhibit moisture transport, while the dual offshore low-pressure systems can exacerbate ozone accumulation through cross-section transport (Qi et al., 2024).

Further analysis of physiochemical processes demonstrates that chemical production plays a dominant role in ozone formation across all four city clusters. Extreme high temperatures can enhance surface O_3 concentrations through accelerating the chemical kinetic rates of photochemical O_3 production and boosting the emission of BVOCs (Zhou et al., 2025). Notably, horizontal transport exhibits a 38 % positive contribution in BTH, while showing significant negative contributions in the other three regions, particularly in YRD and SCB. Vertical transport and mixing processes show relatively minor impacts. These findings highlight the necessity of considering cross-section transport and implementing regional joint prevention and control strategies for effective ozone pollution mitigation.

In summary, all the four city clusters generally demonstrate a common meteorological template during HW days conducive to ozone generation, i.e., elevated temperatures, reduced humidity, enhanced solar radiation, and minimal cloud cover. Crucially, the dynamic behavior of the WPSH (northward migration/westward extension) and its interaction with local circulation systems emerge as the primary drivers of spatial heterogeneity in ozone anomalies. Particularly, for surface ozone in PRD, typhoon activity can also make a significant contribution though cross-section transport. These findings provide critical insights into the mechanistic differences underlying ozone pollution during HWs for major city clusters in China. In future scenarios, while anthropogenic emissions are projected to decline with effective control measures, extreme heat events will likely become more frequent and intense. Our results provide a scientific basis for ozone pollution mitigation strategies under increasing heatwave conditions.

Rapid urbanization in China has led to high anthropogenic precursor emissions and urban heat island effects, both of which may intensify the co-occurrence of ozone pollution and heat extremes (Wu et al., 2024; Qin et al., 2025). As highlighted by Wu et al. (2024) and Qin et al. (2025), evaporative AVOC emissions tend to increase during high-temperature episodes, which can substantially enhance regional ozone production, particularly in urban areas. However, the response of AVOC emissions to temperature changes is not included in GEOS-Chem. Thus, the GEOS-Chem simulations may underestimate the magnitude of ozone enhancement during heatwaves, especially over major city clusters. Moreover, we acknowledge that the GEOS-Chem model may exhibit a certain tendency to underestimate peak ozone concentrations, which introduces some uncertainty into our findings regarding the magnitude of the ozone increase (Jiang et al., 2021). Nevertheless, the consistent patterns observed across different regions and confirmed by observations suggest that the co-occurrence is a robust feature. GEOS-Chem reasonably reproduces the increase in MDA8 O_3 during HWs, although the simulated magnitudes are smaller than those observed. This discrepancy likely reflects uncertainties associated with emission inventories, chemical schemes, and the relatively coarse model resolution, all of which can affect the representation of ozone–heatwave interactions (Jiang et al., 2021; Li et al., 2024b). In particular, the nested-grid capability of GEOS-Chem ($0.5^\circ \times 0.625^\circ$) allows regional analysis

while maintaining global consistency, which is especially important for East Asia where transboundary pollution transport plays a critical role (Chen et al., 2009; Li et al., 2023).

Although GEOS-Chem has the unique advantage of being a global 3-D model that can consistently represent long-range transport, stratosphere-troposphere exchange, and background chemical fields (Bey et al., 2001), its coarse resolution limits the ability to capture the strong spatial heterogeneity between megacities and surrounding urban clusters (Chen et al., 2023), especially for the representation of BVOC emissions. BVOC emissions are highly localized and strongly modulated by urban land use and meteorological conditions (Liu et al., 2022a; Ma et al., 2023). Regional chemistry-climate models have been employed to overcome this limitation by explicitly resolving boundary layer dynamics, land-atmosphere feedback, and localized emission processes (Zhang et al., 2021; Xu et al., 2025; Wang et al., 2025b). For instance, WRF-Chem simulations have demonstrated that urbanization and enhanced BVOC emissions from urban greening can substantially modify ozone formation in PRD and YRD (Zhang et al., 2021; Wu et al., 2023). Therefore, integrating regional-scale modeling frameworks with global chemistry-climate models will be essential to better quantify the nonlinear response of ozone to BVOC emissions under future emission and climate scenarios.

CRediT authorship contribution statement

Yu Song: Writing – review & editing, Writing – original draft, Visualization, Validation, Software, Methodology, Formal analysis. **Pinya Wang:** Writing – review & editing, Supervision, Resources, Conceptualization. **Yang Yang:** Writing – review & editing, Resources, Investigation. **Jianping Tang:** Writing – review & editing, Resources, Conceptualization. **Hong Liao:** Writing – review & editing, Resources, Project administration.

Declaration of competing interest

The authors declare that they have no known competing financial interests or personal relationships that could have appeared to influence the work reported in this paper.

Acknowledgements

This study was supported by the National Natural Science Foundation of China (Grant 42293323, 42521006 and 42475032), and the Natural Science Foundation of Jiangsu Province (Grant BK20241902).

Appendix A. Supplementary data

Supplementary data to this article can be found online at https://doi.org/10.1016/j.atmosres.2025.108580.

Data availability

Hourly O_3 concentrations are obtained from the public website of the China National Environmental Monitoring Centre (http://www.cnemc.cn/en/, CNEMC). The ERA5 reanalysis is available at https://doi.org/10.24381/cds.bd0915c6. The GEOS-Chem model is available at http://www.geos-chem.org.

References

Arjomandi, M., Balmes, J.R., Frampton, M.W., Bromberg, P., Rich, D.Q., Stark, P., Alexis, N.E., Costantini, M., Hollenbeck-Pringle, D., Dagincourt, N., Hazucha, M.J., 2018. Respiratory responses to ozone exposure. Moses (the multicenter ozone study in older subjects). Am. J. Respir. Crit. Care Med. 197 (10), 1319–1327. https://doi.org/10.1164/rccm.201708-1613oc.

Atkinson, R., 2000. Atmospheric chemistry of VOCs and NOx. Atmos. Environ. 34 (12–14), 2063–2101. https://doi.org/10.1016/S1352-2310(99)00460-4.

Barriopedro, D., Fischer, E.M., Luterbacher, J., Trigo, R.M., García-Herrera, R., 2011. The hot summer of 2010: redrawing the temperature record map of Europe. Science 332 (6026), 220–224. https://doi.org/10.1126/science.1201224.

Bey, I., Jacob, D.J., Yantosca, R.M., Logan, J.A., Field, B.D., Fiore, A.M., Li, Q., Liu, H.Y., Mickley, L.J., Schultz, M.G., 2001. Global modeling of tropospheric chemistry with assimilated meteorology: model description and evaluation. J. Geophys. Res. 106 (D19), 23073–23095. https://doi.org/10.1029/2001JD000807.

Booker, F., Muntifering, R., Mcgrath, M., Burkey, K., Decoteau, D., Fiscus, E., Manning, W., Krupa, S., Chappelka, A., Grantz, D., 2009. The ozone component of global change: potential effects on agricultural and horticultural plant yield, product quality and interactions with invasive species. J. Integr. Plant Biol. 51, 337–351. https://doi.org/10.1111/j.1744-7909.2008.00805.x.

Chen, D., Wang, Y., McElroy, M.B., He, K., Yantosca, R.M., Le Sager, P., 2009. Regional CO pollution and export in China simulated by the high-resolution nested-grid GEOS-Chem model. Atmos. Chem. Phys. 9 (11), 3825–3839. https://doi.org/10.5194/acp-9-3825-2009.

Chen, H., Zhao, L., Cheng, L., Zhang, Y., Wang, H., Gu, K., Bao, J., Yang, J., Liu, Z., Huang, J., Chen, Y., Gao, X., Xu, Y., Wang, C., Cai, W., Gong, P., Luo, Y., Liang, W., Huang, C., 2022. Projections of heatwave-attributable mortality under climate change and future population scenarios in China. Lancet Reg. Health West. Pac. 28, 100582. https://doi.org/10.1016/j.lanwpc.2022.100582.

Chen, X., Wang, M., He, T.-L., Jiang, Z., Zhang, Y., Zhou, L., Liu, J., Liao, H., Worden, H., Jones, D., Chen, D., Tan, Q., Shen, Y., 2023. Data- and model-based urban O_3 responses to NOx changes in China and the United States. J. Geophys. Res. Atmos. 128 (20), e2022JD038228. https://doi.org/10.1029/2022JD038228.

Dang, R., Liao, H., Fu, Y., 2021. Quantifying the anthropogenic and meteorological influences on summertime surface ozone in China over 2012–2017. Sci. Total Environ. 754, 142394. https://doi.org/10.1016/j.scitotenv.2020.142394.

Ding, T., Ke, Z., 2015. Characteristics and changes of regional wet and dry heat wave events in China during 1960–2013. Theor. Appl. Climatol. 122, 651–665. https://doi.org/10.1007/s00704-014-1322-9.

Ding, A., Huang, X., Fu, C., 2017. Air pollution and weather interaction in East Asia. In: Oxford Research Encyclopedias: Environmental Science. https://doi.org/10.1093/acefore/9780199389414.013.536.

Feng, Z., Kobayashi, K., 2009. Assessing the impacts of current and future concentrations of surface ozone on crop yield with meta-analysis. Atmos. Environ. 43 (8), 1510–1519. https://doi.org/10.1016/j.atmosenv.2008.11.033.

Feng, Z., Hu, E., Wang, X., Jiang, L., Liu, X., 2015. Ground-level O_3 pollution and its impacts on food crops in China: a review. Environ. Pollut. 199, 42–48. https://doi.org/10.1016/j.envpol.2015.01.016.

Fleming, Z.L., Doherty, R.M., Von Schneidemesser, E., Malley, C.S., Cooper, O.R., Pinto, J.P., Colette, A., Xu, X., Simpson, D., Schultz, M.G., Lefohn, A.S., Hamad, S., Moolla, R., Solberg, S., Feng, Z., 2018. Tropospheric ozone assessment report: present-day ozone distribution and trends relevant to human health. Elem. Sci. Anth. 6 (1), 12. https://doi.org/10.1525/elementa.273.

Gao, J., Yang, Y., Wang, H., Wang, P., Li, B., Li, J., Wei, J., Gao, M., Liao, H., 2023. Climate responses in China to domestic and foreign aerosol changes due to clean air actions during 2013–2019. npj Clim. Atmos. Sci. 6 (1), 160. https://doi.org/10.1038/s41612-023-00488-y.

Gelaro, R., McCarty, W., Suárez, M.J., Todling, R., Molod, A., Takacs, L., Randles, C.A., Darmenov, A., Bosilovich, M.G., Reichle, R., Wargan, K., Coy, L., Cullather, R., Draper, C., Akella, S., Buchard, V., Conaty, A., Da Silva, A.M., Gu, W., Kim, G., Koster, R., Lucchesi, R., Merkova, D., Nielsen, J., Partyka, G., Pawson, S., Putman, W., Rienecker, M., Schubert, S.D., Sienkiewicz, M., Zhao, B., 2017. The modern-era retrospective analysis for research and applications, version 2 (MERRA-2). J. Clim. 30, 5419–5454. https://doi.org/10.1175/JCLI-D-16-0758.1.

Gong, C., Liao, H., 2019. A typical weather pattern for ozone pollution events in North China. Atmos. Chem. Phys. 19, 13725–13740. https://doi.org/10.5194/acp-19-13725-2019.

Guenther, A.B., Jiang, X., Heald, C.L., Sakulyanontvittaya, T., Duhl, T., Emmons, L.K., Wang, X., 2012. The model of emissions of gases and aerosols from nature version 2.1 (MEGAN2.1): an extended and updated framework for modeling biogenic emissions. Geosci. Model Dev. 5, 1471–1492. https://doi.org/10.5194/gmd-5-1471-2012.

Hoesly, R.M., Smith, S.J., Feng, L., Klimont, Z., Janssens-Maenhout, G., Pitkanen, T., Seibert, J.J., Vu, L., Andres, R.J., Bolt, R.M., Bond, T.C., Dawidowski, L., Kholod, N., Kurokawa, J.-I., Li, M., Liu, L., Lu, Z., Moura, M.C.P., O'Rourke, P.R., Zhang, Q., 2018. Historical (1750–2014) anthropogenic emissions of reactive gases and aerosols from the community emissions data system (CEDS). Geosci. Model Dev. 11, 369–408. https://doi.org/10.5194/gmd-11-369-2018.

Intergovernmental Panel on Climate Change (IPCC), 2023. Weather and climate extreme events in a changing climate. In: Climate Change 2021 – The Physical Science Basis: Working Group I Contribution to the Sixth Assessment Report of the Intergovernmental Panel on Climate Change. Cambridge University Press, pp. 1513–1766. https://doi.org/10.1017/9781009157896.013.

Jha, R., Perkins-Kirkpatrick, S.E., Singh, D., Kimutai, J., Libonati, R., Mondal, A., 2025. Extreme terrestrial heat in 2024. Nat. Rev. Earth Environ. 6, 234–236. https://doi.org/10.1038/s43017-025-00661-2.

Jia, H., Guo, Y., Luo, H., Meng, X., Zhang, L., Yu, K., Zheng, X., Sun, Y., Hu, W., Wu, Z., Chen, R., Sun, X., 2024. Association of long-term ozone air pollution and age-related macular degeneration in older Chinese population. Sci. Total Environ. 912, 169145. https://doi.org/10.1016/j.scitotenv.2023.169145.

Jiang, Z., Li, J., Lu, X., Gong, C., Zhang, L., Liao, H., 2021. Impact of western Pacific subtropical high on ozone pollution over eastern China. Atmos. Chem. Phys. 21, 2601–2613. https://doi.org/10.5194/acp-21-2601-2021.

Kalisa, E., Fadlallah, S., Amani, M., Nahayo, L., Habiyaremye, G., 2018. Temperature and air pollution relationship during heatwaves in Birmingham, UK. Sustain. Cities Soc. 43, 111–120. https://doi.org/10.1016/j.scs.2018.08.033.

Lau, N.C., Nath, M.J., 2014. Model simulation and projection of European heat waves in present-day and future climates. J. Clim. 27, 3713–3730. https://doi.org/10.1175/JCLI-D-13-00284.1.

Li, Q., Liu, X., Zhang, H., Peterson, T.C., Easterling, D.R., 2004. Detecting and adjusting temporal inhomogeneity in Chinese mean surface air temperature data. Adv. Atmos. Sci. 21, 260–268. https://doi.org/10.1007/bf02915712.

Li, K., Jacob, D.J., Liao, H., Shen, L., Zhang, Q., Bates, K.H., 2019. Anthropogenic drivers of 2013-2017 trends in summer surface ozone in China. Proc. Natl. Acad. Sci. USA 116 (2), 422–427. https://doi.org/10.1073/pnas.1812168116.

Li, H., Yang, Y., Jin, J., Wang, H., Li, K., Wang, P., Liao, H., 2023. Climate-driven deterioration of future ozone pollution in Asia predicted by machine learning with multi-source data. Atmos. Chem. Phys. 23 (2), 1131–1145. https://doi.org/10.5194/acp-23-1131-2023.

Li, M., Huang, X., Yan, D., Lai, S., Zhang, Z., Zhu, L., Lu, Y., Jiang, X., Wang, N., Wang, T., Song, Y., Ding, A., 2024a. Coping with the concurrent heatwaves and ozone extremes in China under a warming climate. Sci. Bull. (Beijing) 69 (18), 2938–2947. https://doi.org/10.1016/j.scib.2024.05.034.

Li, M., Yang, Y., Wang, H., Wang, P., Liao, H., 2024b. Unique impacts of strong and westward-extended western Pacific subtropical high on ozone pollution over eastern China. Environ. Pollut. 358, 124515. https://doi.org/10.1016/j.envpol.2024.124515.

Li, S., Gao, Y., Zhang, J., Hong, C., Zhang, S., Chen, D., Wild, O., Feng, Z., Xu, Y., Guo, X., Kou, W., Yan, F., Ma, M., Yao, X., Gao, H., Davis, S.J., 2025. Mitigating climate change and ozone pollution will improve chinese food security. One Earth 8 (2), 101166. https://doi.org/10.1016/j.oneear.2024.12.002.

Lin, M., Horowitz, L., Xie, Y., Paulot, F., Malyshev, S., Shevliakova, E., Finco, A., Gerosa, G., Kubistin, D., Pilegaard, K., 2020. Vegetation feedbacks during drought exacerbate ozone air pollution extremes in Europe. Nat. Clim. Chang. 10, 444–451. https://doi.org/10.1038/s41558-020-0743-y.

Liu, S., Sahu, S.K., Zhang, S., Liu, S., Sun, Y., Liu, X., Xing, J., Zhao, B., Zhang, H., Wang, S., 2022a. Impact of climate-driven land-use change on O_3 and PM pollution by driving BVOC emissions in China in 2050. Atmosphere 13, 1086. https://doi.org/10.3390/atmos13071086.

Liu, S., Zhang, Y., Ma, R., Liu, X., Liang, J., Lin, H., Shen, P., Zhang, J., Lu, P., Tang, X., Li, T., Gao, P., 2022b. Long-term exposure to ozone and cardiovascular mortality in a large Chinese cohort. Environ. Int. 165, 107280. https://doi.org/10.1016/j.envint.2022.107280.

Lu, X., Zhang, L., Chen, Y., Zhou, M., Zheng, B., Li, K., Liu, Y., Lin, J., Fu, T.-M., Zhang, Q., 2019. Exploring 2016–2017 surface ozone pollution over China: source contributions and meteorological influences. Atmos. Chem. Phys. 19, 8339–8361. https://doi.org/10.5194/acp-19-8339-2019.

Lu, X., Zhang, L., Wang, X., Gao, M., Li, K., Zhang, Y., Yue, X., Zhang, Y., 2020. Rapid increases in warm-season surface ozone and resulting health impact over China since 2013. Environ. Sci. Technol. Lett. 7, 240–247. https://doi.org/10.1021/acs.estlett.0c00171.

Luo, M., Lau, N.-C., 2017. Heat waves in Southern China: synoptic behavior, long-term change, and urbanization effects. J. Clim. 30, 703–720. https://doi.org/10.1175/JCLI-D-16-0269.1.

Ma, M., Gao, Y., Wang, Y., Zhang, S., Leung, L.R., Liu, C., Wang, S., Zhao, B., Chang, X., Su, H., Zhang, T., Sheng, L., Yao, X., Gao, H., 2019. Substantial ozone enhancement over the North China Plain from increased biogenic emissions due to heat waves and land cover in summer 2017. Atmos. Chem. Phys. 19, 12195–12207. https://doi.org/10.5194/acp-19-12195-2019.

Ma, J., Zhu, S., Wang, S., Wang, P., Chen, J., Zhang, H., 2023. Impacts of land cover changes on biogenic emission and its contribution to ozone and secondary organic aerosol in China. Atmos. Chem. Phys. 23, 4311–4325. https://doi.org/10.5194/acp-23-4311-2023.

Mao, J., Paulot, F., Jacob, D.J., Cohen, R.C., Crounse, J.D., Wennberg, P.O., Keller, C.A., Hudman, R.C., Barkley, M.P., Horowitz, L.W., 2013. Ozone and organic nitrates over the eastern United States: sensitivity to isoprene chemistry. J. Geophys. Res. Atmos. 118, 11256–11268. https://doi.org/10.1002/jgrd.50817.

McLinden, C.A., Olsen, S.C., Hannegan, B., Wild, O., Prather, M.J., Sundet, J., 2000. Stratospheric ozone in 3-D models: a simple chemistry and the cross-tropopause flux. J. Geophys. Res. 105 (D11), 14653–14665. https://doi.org/10.1029/2000JD900124.

Meehl, G.A., Tebaldi, C., 2004. More intense, more frequent, and longer lasting heat waves in the 21st century. Science 305, 994–997. https://doi.org/10.1126/science.1098704.

Ni, R., Lin, J., Yan, Y., Lin, W., 2018. Foreign and domestic contributions to springtime ozone over China. Atmos. Chem. Phys. 18, 11447–11469. https://doi.org/10.5194/acp-18-11447-2018.

Ni, Y., Yang, Y., Wang, H., Li, H., Li, M., Wang, P., Li, K., Liao, H., 2024. Contrasting changes in ozone during 2019-2021 between eastern and the other regions of China attributed to anthropogenic emissions and meteorological conditions. Sci. Total Environ. 908, 168272. https://doi.org/10.1016/j.scitotenv.2023.168272.

Ouyang, S., Deng, T., Liu, R., Chen, J., He, G., Leung, J.C.-H., Wang, N., Liu, S.C., 2022. Impact of a subtropical high and a typhoon on a severe ozone pollution episode in the Pearl River Delta, China. Atmos. Chem. Phys. 22, 10751–10767. https://doi.org/10.5194/acp-22-10751-2022.

Perkins, S.E., Alexander, L.V., 2013. On the measurement of heat waves. J. Clim. 26, 4500–4517. https://doi.org/10.1175/JCLI-D-12-00383.1.

Pu, X., Wang, T.J., Huang, X., Melas, D., Zanis, P., Papanastasiou, D.K., Poupkou, A., 2017. Enhanced surface ozone during the heat wave of 2013 in Yangtze River Delta region, China. Sci. Total Environ. 603-604, 807–816. https://doi.org/10.1016/j.scitotenv.2017.03.056.

Pye, H.O.T., Liao, H., Wu, S., Mickley, L.J., Jacob, D.J., Henze, D.K., Seinfeld, J.H., 2009. Effect of changes in climate and emissions on future sulfate-nitrate-ammonium aerosol levels in the United States. J. Geophys. Res. Atmos. 114, 2008JD010701. https://doi.org/10.1029/2008JD010701.

Qi, C., Wang, P., Yang, Y., Li, H., Zhang, H., Ren, L., Jin, X., Zhan, C., Tang, J., Liao, H., 2024. Impacts of tropical cyclone–heat wave compound events on surface ozone in eastern China: comparison between the Yangtze River and Pearl River deltas. Atmos. Chem. Phys. 24, 11775–11789. https://doi.org/10.5194/acp-24-11775-2024.

Qin, M., She, Y., Wang, M., Wang, H., Chang, Y., Tan, Z., An, J., Huang, J., Yuan, Z., Lu, J., Wang, Q., Liu, C., Liu, Z., Xie, X., Li, J., Liao, H., Pye, H.O.T., Huang, C., Guo, S., Hu, M., Zhang, Y., Jacob, D.J., Hu, J., 2025. Increased urban ozone in heatwaves due to temperature-induced emissions of anthropogenic volatile organic compounds. Nat. Geosci. 18, 50–56. https://doi.org/10.1038/s41561-024-01608-w.

Sherwen, T., Schmidt, J.A., Evans, M.J., Carpenter, L.J., Großmann, K., Eastham, S.D., Jacob, D.J., Dix, B., Koenig, T.K., Sinreich, R., Ortega, I., Volkamer, R., Saiz-Lopez, A., Prados-Roman, C., Mahajan, A.S., Ordóñez, C., 2016. Global impacts of tropospheric halogens (Cl, Br, I) on oxidants and composition in GEOS-Chem. Atmos. Chem. Phys. 16, 12239–12271. https://doi.org/10.5194/acp-16-12239-2016.

Shu, L., Xie, M., Wang, T., Gao, D., Chen, P., Han, Y., Li, S., Zhuang, B., Li, M., 2016. Integrated studies of a regional ozone pollution synthetically affected by subtropical high and typhoon system in the Yangtze River Delta region, China Atmos. Chem. Phys. 16, 15801–15819. https://doi.org/10.5194/acp-16-15801-2016.

Sillman, S., 1999. The relation between ozone, NO_x and hydrocarbons in urban and polluted rural environments. Atmos. Environ. 33, 1821–1845. https://doi.org/10.1016/S1352-2310(98)00345-8.

Steinbrecht, W., Kubistin, D., Plass-Dülmer, C., Davies, J., Tarasick, D.W., von der Gathen, P., Deckelmann, H., Jepsen, N., Kivi, R., Lyall, N., Palm, M., Notholt, J., Kois, B., Oelsner, P., Allaart, M., Piters, A., Gill, M., Van Malderen, R., Delcloo, A.W., Sussmann, R., Mahieu, E., Servais, C., Romanens, G., Stübi, R., Ancellet, G., Godin-Beekmann, S., Yamanouchi, S., Strong, K., Johnson, B., Cullis, P., Petropavlovskikh, I., Hannigan, J.W., Hernandez, J.L., Diaz Rodriguez, A., Nakano, T., Chouza, F., Leblanc, T., Torres, C., Garcia, O., Röhling, A.N., Schneider, M., Blumenstock, T., Tully, M., Paton-Walsh, C., Jones, N., Querel, R., Strahan, S., Stauffer, R.M., Thompson, A.M., Inness, A., Engelen, R., Chang, K.L., Cooper, O.R., Cooper, O.R., 2021. COVID-19 crisis reduces free tropospheric ozone across the Northern Hemisphere. Geophys. Res. Lett. 48 (5), e2020GL091987. https://doi.org/10.1029/2020GL091987.

Tong, S., Wang, X.Y., Barnett, A.G., 2010. Assessment of heat-related health impacts in Brisbane, Australia: comparison of different heatwave definitions. PLoS One 5 (8), e12155. https://doi.org/10.1371/journal.pone.0012155.

Trainer, M., Parrish, D., Goldan, P., Roberts, J., Fehsenfeld, F., 2000. Review of observation-based analysis of the regional factors influencing ozone concentrations. Atmos. Environ. 34, 2045–2061. https://doi.org/10.1016/S1352-2310(99)00459-8.

Van der Werf, G.R., Randerson, J.T., Giglio, L., van Leeuwen, T.T., Chen, Y., Rogers, B.M., Mu, M., van Marle, M.J.E., Morton, D.C., Collatz, G.J., Yokelson, R.J., Kasibhatla, P.S., 2017. Global fire emissions estimates during 1997–2016. Earth Syst. Sci. Data 9, 697–720. https://doi.org/10.5194/essd-9-697-2017.

Varotsos, K.V., Giannakopoulos, C., Tombrou, M., 2019. Ozone-temperature relationship during the 2003 and 2014 heatwaves in Europe. Reg. Environ. Chang. 19, 1653–1665. https://doi.org/10.1007/s10113-019-01498-4.

Wang, X.Y., Barnett, A.G., Yu, W., FitzGerald, G., Tippett, V., Aitken, P., Neville, G., McRae, D., Verrall, K., Tong, S., 2012. The impact of heatwaves on mortality and emergency hospital admissions from non-external causes in Brisbane, Australia. Occup. Environ. Med. 69 (3), 163–169. https://doi.org/10.1136/oem.2010.062141.

Wang, P., Tang, J., Sun, X., Wang, S., Wu, J., Dong, X., Fang, J., 2017. Heatwaves in China: definitions, leading patterns and connections to large-scale atmospheric circulation and SSTs. J. Geophys. Res. Atmos. 122, 10679–10699. https://doi.org/10.1002/2017JD027180.

Wang, P., Hui, P., Xue, D., Tang, J., 2019a. Future projection of heat waves over China under global warming within the CORDEX-EA-II project. Clim. Dyn. 53, 957–973. https://doi.org/10.1007/s00382-019-04621-7.

Wang, P., Leung, L.R., Lu, J., Song, F., Tang, J., 2019b. Extreme wet-bulb temperatures in China: the significant role of moisture. J. Geophys. Res.-Atmos. 124, 11944–11960. https://doi.org/10.1029/2019JD031477.

Wang, W., Parrish, D.D., Wang, S., Bao, F., Ni, R., Li, X., Yang, S., Wang, H., Cheng, Y., Su, H., 2022a. Long-term trend of ozone pollution in China during 2014–2020: distinct seasonal and spatial characteristics and ozone sensitivity. Atmos. Chem. Phys. 22, 8935–8949. https://doi.org/10.5194/acp-22-8935-2022.

Wang, P., Yang, Y., Li, H., Chen, L., Dang, R., Xue, D., Li, B., Tang, J., Leung, L.R., Liao, H., 2022b. North China Plain as a hot spot of ozone pollution exacerbated by extreme high temperatures. Atmos. Chem. Phys. 22, 4705–4719. https://doi.org/10.5194/acp-22-4705-2022.

Wang, P., Yang, Y., Xue, D., Qu, Y., Tang, J., Leung, L.R., Liao, H., 2023a. Increasing compound hazards of tropical cyclones and heatwaves over southeastern coast of China under climate warming. J. Clim. 36 (7), 2243–2257. https://doi.org/10.1175/JCLI-D-22-0279.1.

Wang, Y., Zhao, Y., Liu, Y., Jiang, Y., Zheng, B., Xing, J., Liu, Y., Wang, S., Nielsen, C.P., 2023b. Sustained emission reductions have restrained the ozone pollution over China. Nat. Geosci. 16, 967–974. https://doi.org/10.1038/s41561-023-01284-2.

Wang, N., Du, Y., Chen, D., Meng, H., Chen, X., Zhou, L., Shi, G., Zhan, Y., Feng, M., Li, W., Chen, M., Li, Z., Yang, F., 2024a. Spatial disparities of ozone pollution in the Sichuan Basin spurred by extreme, hot weather. Atmos. Chem. Phys. 24, 3029–3042. https://doi.org/10.5194/acp-24-3029-2024.

Wang, J., Li, J., Li, X., Wang, D., Fang, C., 2024b. Relationship between ozone and air temperature in future conditions: a case study in Sichuan basin, China. Environ. Pollut. 343, 123276. https://doi.org/10.1016/j.envpol.2023.123276.

Wang, H., Nagalingam, S., Welch, A.M., Leong, C., Czimczik, C.I., Guenther, A.B., 2024c. Heat waves may trigger unexpected surge in aerosol and ozone precursor emissions from sedges in urban landscapes. Proc. Natl. Acad. Sci. USA 121 (45), e2412817121. https://doi.org/10.1073/pnas.2412817121.

Wang, N., Wang, H., Huang, X., Chen, X., Zou, Y., Deng, T., Li, T., Lyu, X., Yang, F., 2024d. Extreme weather exacerbates ozone pollution in the Pearl River Delta, China: role of natural processes. Atmos. Chem. Phys. 24, 1559–1570. https://doi.org/10.5194/acp-24-1559-2024.

Wang, L., Chen, B., Ouyang, J., Mu, Y., Zhen, L., Yang, L., Xu, W., Tang, L., 2025a. Causal-inference machine learning reveals the drivers of China's 2022 ozone rebound. Environ. Sci. Ecotechnol. 24, 100524. https://doi.org/10.1016/j.ese.2025.100524.

Wang, N., Liu, S., Xu, J., Wang, Y., Li, C., Xie, Y., Lu, H., Yang, F., 2025b. Climate-driven biogenic emissions alleviate the impact of human-made emission reductions on O_3 control in the Pearl River Delta region, southern China. Atmos. Chem. Phys. 25, 8859–8870. https://doi.org/10.5194/acp-25-8859-2025.

Wu, L., Yang, L., Zhang, Y., Wu, G., Chen, W., Deng, S., Situ, S., Chang, M., Wang, X., 2023. Prediction of ozone pollution impacted by vegetation planning in the Pearl River Delta, China. Atmos. Environ. 309, 119936. https://doi.org/10.1016/j.atmosenv.2023.119936.

Wu, W., Fu, T.M., Arnold, S.R., Spracklen, D.V., Zhang, A., Tao, W., Wang, X., Hou, Y., Mo, J., Chen, J., Li, Y., Feng, X., Lin, H., Huang, Z., Zheng, J., Shen, H., Zhu, L., Wang, C., Ye, J., Yang, X., 2024. Temperature-dependent evaporative anthropogenic VOC emissions significantly exacerbate regional ozone pollution. Environ. Sci. Technol. 58 (12), 5430–5441. https://doi.org/10.1021/acs.est.3c09122.

Xie, Y., Zhou, Z., Sun, Q., Zhao, M., Pu, J., Li, Q., Sun, Y., Dai, H., Li, T., 2024. Social-economic transitions and vulnerability to extreme temperature events from 1960 to 2020 in Chinese cities. iScience 27 (3), 109066. https://doi.org/10.1016/j.isci.2024.109066.

Xu, J., Silver, B., Tang, R., Wang, N., Huang, X., Ding, A., Arnold, S.R., 2025. A model assessment of the relationship between urban greening and ozone air quality in China: a study of three metropolitan regions. npj Clim. Atmos. Sci. 8, 184. https://doi.org/10.1038/s41612-025-01054-4.

Yan, D., Jin, Z., Zhou, Y., Li, M., Zhang, Z., Wang, T., Zhuang, B., Li, S., Xie, M., 2024. Anthropogenically and meteorologically modulated summertime ozone trends and their health implications since China's clean air actions. Environ. Pollut. 343, 123234. https://doi.org/10.1016/j.envpol.2023.123234.

Yang, Y., Liao, H., Li, J., 2014. Impacts of the East Asian summer monsoon on interannual variations of summertime surface-layer ozone concentrations over China. Atmos. Chem. Phys. 14, 6867–6879. https://doi.org/10.5194/acp-14-6867-2014.

Yang, Y., Li, M., Wang, H., Li, H., Wang, P., Li, K., Gao, M., Liao, H., 2022. ENSO modulation of summertime tropospheric ozone over China. Environ. Res. Lett. 17, 034020. https://doi.org/10.1088/1748-9326/ac54cd.

Yang, Z., Li, Z., Cheng, F., Lv, Q., Li, K., Zhang, T., Zhou, Y., Zhao, B., Xue, W., Wei, J., 2025. Two-decade surface ozone (O_3) pollution in China: enhanced fine-scale estimations and environmental health implications. Remote Sens. Environ. 317, 114459. https://doi.org/10.1016/j.rse.2024.114459.

Yin, H., Lu, X., Sun, Y., Li, K., Gao, M., Zheng, B., Liu, C., 2021. Unprecedented decline in summertime surface ozone over eastern China in 2020 comparably attributable to anthropogenic emission reductions and meteorology. Environ. Res. Lett. 16 (12), 124069. https://doi.org/10.1088/1748-9326/ac3e22.

You, Q., Jiang, Z., Kong, L., Wu, Z., Bao, Y., Kang, S., Pepin, N., 2017. A comparison of heat wave climatologies and trends in China based on multiple definitions. Clim. Dyn. 48, 3975–3989. https://doi.org/10.1007/s00382-016-3315-0.

Zhang, Q., Zheng, Y., Tong, D., Shao, M., Wang, S., Zhang, Y., Xu, X., Wang, J., He, H., Liu, W., Ding, Y., Lei, Y., Li, J., Wang, Z., Zhang, X., Wang, Y., Cheng, J., Liu, Y., Shi, Q., Yan, L., Geng, G., Hong, C., Li, M., Liu, F., Zheng, B., Cao, J., Ding, A., Gao, J., Fu, Q., Huo, J., Liu, B., Liu, Z., Yang, F., He, K., Hao, J., 2019. Drivers of improved PM2.5 air quality in China from 2013 to 2017. Proc. Natl. Acad. Sci. USA 116 (49), 24463–24469. https://doi.org/10.1073/pnas.1907956116.

Zhang, M., Zhao, C., Yang, Y., Du, Q., Shen, Y., Lin, S., Gu, D., Su, W., Liu, C., 2021. Modeling sensitivities of BVOCs to different versions of MEGAN emission schemes in WRF-Chem (v3.6) and its impacts over eastern China. Geosci. Model Dev. 14, 6155–6175. https://doi.org/10.5194/gmd-14-6155-2021.

Zhao, S., Yu, Y., Yin, D., Qin, D., He, J., Dong, L., 2018. Spatial patterns and temporal variations of six criteria air pollutants during 2015 to 2017 in the city clusters of Sichuan Basin, China. Sci. Total Environ. 624, 540–557. https://doi.org/10.1016/j.scitotenv.2017.12.172.

Zhou, X., Li, M., Huang, X., Liu, T., Zhang, H., Qi, X., Wang, Z., Qin, Y., Geng, G., Wang, J., Chi, X., Ding, A., 2025. Urban meteorology–chemistry coupling in compound heat–ozone extremes. Nat. Cities. https://doi.org/10.1038/s44284-025-00302-1.

Zhu, S., Ma, J., Wang, S., Sun, S., Wang, P., Zhang, H., 2023. Shifts of formation regimes and increases of atmospheric oxidation led to ozone increase in North China Plain and Yangtze River Delta from 2016 to 2019. J. Geophys. Res. Atmos. 128 (13). https://doi.org/10.1029/2022jd038373.